Constrained Safe Cooperative Maneuvering of Autonomous Surface Vehicles: A Control Barrier Function Approach

Wentao Wu, *Graduate Student Member, IEEE,* Yibo Zhang, *Member, IEEE,* Zhenhua Li, Jun-Guo Lu, and Weidong Zhang, *Senior Member, IEEE*

***Abstract*—This paper investigates a constrained safe cooperative maneuvering method for a group of autonomous surface vehicles (ASVs) with performance-quantized indices in an obstacle-loaded environment. Specifically, an avoidance-tolerant prescribed performance (ATPP) with one-sided tunnel bounds is designed to predetermine the cooperative maneuvering performance of multiple ASVs. Next, an auxiliary system is constructed to modify performance bounds of ATPP for tolerating possible collision avoidance actions of ASVs. In the guidance loop, nominal surge and yaw guidance laws are developed using the ATPP-based transformed relative distance and heading errors. A barrier-certified yaw velocity protocol is proposed by formulating a quadratic optimization problem, which unifies the nominal yaw guidance law and CBF-based collision-free constraints. In the control loop, two prescribed-time disturbance observers (PTDOs) are devised to estimate unknown external disturbances in the surge and yaw directions. The antidisturbance control laws are designed to track the guidance signals. By the stability and safety analysis, it is proved that error signals of the proposed closed-loop system are bounded and the multi-ASV system is input-to-state safe. Finally, simulation results are used to demonstrate the effectiveness of the presented constrained safe cooperative maneuvering method.**

***Index Terms*—Underactuated autonomous surface vehicles, avoidance-tolerant prescribed performance, control barrier function, cooperative maneuvering, safety-critical control.**

I. Introduction

In recent years, autonomous surface vehicle (ASV), as a kind of intelligent marine vehicles without human intervention, has gained increasing attentions due to promising maritime applications, such as ocean exploration, surveillance, mapping, and transportation, to name a few [1]–[5]. To enhance the capability and effectiveness of accomplishing missions, a group of ASVs are driven to implement the cooperative operation for a collaborative behavior by sharing their own information with other individuals. The typical cooperative patterns include consensus [6], containment [7], flocking [8], target enclosing [9], target tracking [10], formation [11], [12], etc. The primary challenge of cooperative control lies in devising the control protocol for every ASV to establish and maintain a predefined geometric configuration.

For ASVs in the sea, it is difficult to achieve the cooperation task owing to model nonlinearities, parameter uncertainties, and external disturbances. Consequently, the existing research results on cooperative control have been investigated in [13]–[18]. In [13], [14], the spatial-temporal cooperative control schemes with path maneuvering techniques are proposed based on the approximated vehicle kinetics from echo state network (ESN)-based estimators. In [15], the approximation speed of ESNs is improved by integrating the accelerated learning technique. Besides the adaptive approximation methods [13]–[15], extended state observers (ESOs) are also employed to not only estimate disturbances but also recovery states. In [16], [17], finite-time ESOs (FTESOs) are presented to obtain the fast estimation ability. In [16], an FTESO-based even-triggered control scheme is derived to degrade the communication burden of multi-ASV containment task. In [17], the robust exact differentiator-based FTESO is developed to estimate the velocity information of leader vessel within finite time. In [18], the cooperative dynamic positioning of ASVs with multiple operating points is performed by developing a network-based control scheme under the fixed topology. The aforementioned controllers can force cooperative errors to converge to a residual set. Note that convergence rate and state-steady accuracy of cooperative errors are not explicitly preconfigured to a safety region, which may degrade the multi-ASV system reliability.

To explicitly depict the performance constraints, [19] proposes the prescribed performance control (PPC) for MIMO nonlinear systems to obtain the desired transient and steady-state indices by predetermining behavioral functions. There are many research results on PPC applications to marine vehicle systems [20]–[28]. In [20], by using disturbance observers (DOs), a PPC-based distributed control method is proposed to perform the containment formation of multiple ASVs under unknown external disturbances. In [21], [22], high-gain observers-based adaptive output-feedback control schemes are presented for ASVs with unavailable velocities to achieve performance-prescribed trajectory tracking. In [23], [24], input and output constraints of ASVs are considered in the distributed cooperative control by constructing the adaptive fuzzy state observers. In [25]–[27], the trajectory tracking

This work was supported in part by the National Key R&D Program of China under Grant 2022ZD0119900 and Grant 2022ZD0119903; in part by the Shanghai Science and Technology Program under Grant 22015810300; in part by the Hainan Province Science and Technology Special Fund under Grant ZDYF2021GXJS041; in part by the National Natural Science Foundation of China under Grant U2141234, Grant 62073217, and Grant 52201369; in part by the Hainan Special Ph.D. Scientific Research Foundation of Sanya Yazhou Bay Science and Technology City under Grant HSPHDSRF-2022-01-007; in part by the China Post-Doctoral Science Foundation under Grant 2022M722053; in part by the Oceanic Interdisciplinary Program of Shanghai Jiao Tong University under Grant SL2022PT112. (*Corresponding Authors: Yibo Zhang; Weidong Zhang*.)

Wentao Wu, Yibo Zhang, Zhenhua Li, and Jun-Guo Lu are with the Department of Automation, Shanghai Jiao Tong University, Shanghai 200240, China (e-mail: wentao-wu@sjtu.edu.cn; e-mail: zhang297@sjtu.edu.cn; e-mail: lizhenhuagd@163.com; e-mail: jglu@sjtu.edu.cn).

Weidong Zhang is with the Department of Automation, Shanghai Jiao Tong University, Shanghai 200240, China, and Weidong Zhang is also with the School of Information and Communication Engineering, Hainan University, Haikou 570228, China (e-mail: wdzhang@sjtu.edu.cn).

control of ASVs with prescribed performance and actuator faults are derived using the fault compensation approaches. It should be pointed out that these methods do not address the safety problem of multi-ASV system, i.e. vehicle avoidance and obstacle avoidance.

In an obstacle-loaded ocean, the safe cooperative operation of multiple ASVs is critical and challenging due to encountering vehicles and dynamic/stationary obstacles. Some collision avoidance strategies have been reported including differentiable function [29], vector field [30], potential function [31]–[33], PPC [34], [35], and control barrier functions (CBFs) [36]–[39], to name a few. In [30], a topology-switched containment maneuvering method is devised using the vector field approach for tackling inter-ASV collisions. In [36], [37], [39], CBF-based collision-free protocols are derived by formulating a optimization problem to avoid encountering ASVs and obstacles. In [34], [35], collision-free constraints are incorporated into the PPC control framework, and a leader-follower formation method is designed to not only obtain guaranteed performance but also avoid inter-vehicle collisions. Along with precision and inter-vehicle collision avoidance, [32], [33] also avoid collision with stationary obstacles by introducing potential functions. It is worth noting that these PPC methods [32]–[35] cannot ensure the safety of multi-ASV formation subject to encountering ASVs and dynamic obstacles. Although CBF-based methods can deal with aforementioned collision-free scenarios, transient and state-steady performance of tracking errors are ignored. For existing PPC and CBF methods, it is a difficult task to simultaneously meet performance and safety constraints because inflexible bounds have poor tolerance for fluctuating errors.

Motivated by the above discussions, this paper aims to develop a constrained safe cooperative maneuvering method for multiple underactuated ASVs subject to dynamic and stationary obstacles. The main contributions of this paper are detailed below.

- In contrast to cooperative control methods [13]–[18], [20]–[31], [36]–[39] without simultaneously considering output and safety constraints, this paper develops a constrained safe cooperative maneuvering method for multiple ASVs in an obstacle-loaded environment. Different from [6], [32]–[35], the cooperation safety of the multi-ASV system subject to dynamic obstacles is also guaranteed using the developed yaw velocity protocol based on second-order CBFs.
- In contrast to PPC and TPP methods [20]–[28], [32]–[35], where behavioral functions are possibly violated due to collision avoidance, this paper designs an avoidance-tolerant prescribed performance (ATPP) capable of enlarging or recovering error bounds. The designed ATPP establishes a trade-off mechanism between tracking errors and output constraints by constructing auxiliary systems associated with safety constraints.
- In contrast to DOs and ESOs proposed in [29], [33], [40]–[46] with asymptotic, finite-time, or fixed-time convergence abilities, the prescribed-time DOs (PTDOs) are designed to estimate unknown disturbances within a predefined constant. The setting time of designed PTDOs is independent on initial values.

This paper is organized as follows. Section II introduces preliminaries and problem formulation. Section III designs the constrained safe cooperative maneuvering controller. Section IV gives the stability analysis. Section V provides simulation results. Section VI concludes this paper.

II. Preliminaries and Problem Formulation

A. Preliminaries

1) Notations: Throughout this paper, $\Re^+$, $\Re^m$ and $\Re^{m\times n}$ represents a positive real space, an m-dimensional Euclidean space, and an $m\times n$-dimensional Euclidean space, respectively. 0_m and $0_{m\times n}$ denote an m-dimensional zero vector and a $m\times n$-dimensional zero matrix, respectively. diag$\{\cdots\}$ is a block-diagonal matrix. $\|\cdot\|$ denotes the Euclidean norm of a vector. $\bar{\lambda}(\cdot)$ and $\underline{\lambda}(\cdot)$ represent the minimum and maximum of a symmetric matrix. $\otimes$ denotes a Kronecker product.

2) Graph theory: This paper considers a system containing M ASVs, $(N-M)$ virtual leaders, and one super leader. The information transmission among them can be depicted via a graph $\mathcal{G}=\{\mathcal{N},\mathcal{V},\mathcal{E},\mathcal{A}\}$. $\mathcal{N}=\{n_0,...,n_N\}$ denotes the set of all nodes. $\mathcal{V}=\{\mathcal{V}^F,\mathcal{V}^L,\mathcal{V}^S\}$ is a vertex set with $\mathcal{V}^F=\{n_1,...,n_M\}$, $\mathcal{V}^L=\{n_{M+1},...,n_N\}$, and $\mathcal{V}^S=\{n_0\}$. $\mathcal{E}=\{(n_i,n_j)\in\mathcal{V}\times\mathcal{V}\}$ is an edge set to describe the information flow among nodes n_i and n_j. To depict the neighboring relationship, the neighborhood set of node n_i is defined as $\mathcal{N}_i=\{\mathcal{N}_i^F,\mathcal{N}_i^L,\mathcal{N}_i^S\}$ with $\mathcal{N}_i^F=\{n_j\in\mathcal{V}^F|(n_i,n_j)\in\mathcal{E}\}$, $\mathcal{N}_i^L=\{n_j\in\mathcal{V}^L|(n_i,n_j)\in\mathcal{E}\}$, and $\mathcal{N}_i^S=\{n_j\in\mathcal{V}^S|(n_i,n_j)\in\mathcal{E}\}$. $\mathcal{A}\in\Re^{(N+1)\times(N+1)}$ is an adjacency matrix with $\mathcal{A}=[a_{ij}]$. If node n_i can acquire the information flow from node n_j, i.e. $(n_i,n_j)\in\mathcal{E}$, $a_{ij}=1$, otherwise, $a_{ij}=0$. The graph $\mathcal{V}$ is called as the undirected graph if $a_{ij}=a_{ij}$. $\mathcal{D}\in\Re^{(N+1)\times(N+1)}$ is a degree matrix defined by $\mathcal{D}=\mathrm{diag}\{d_i\}$ with $d_i=\sum_{j\in\mathcal{N}_i}a_{ij}$. A Laplacian matrix $\mathcal{L}\in\Re^{(N+1)\times(N+1)}$ is devised as

$$\mathcal{L}=\mathcal{D}-\mathcal{A}=\begin{bmatrix}0 & 0_M^T & \mathcal{L}_3\\ 0_M & \mathcal{L}_1 & \mathcal{L}_2\\ \mathcal{L}_3^T & \mathcal{L}_2^T & \mathcal{L}_0\end{bmatrix} \tag{1}$$

where $\mathcal{L}_0\in\Re^{(N-M)\times(N-M)}$, $\mathcal{L}_1\in\Re^{M\times M}$, $\mathcal{L}_2\in\Re^{M\times(N-M)}$, and $\mathcal{L}_3\in\Re^{1\times(N-M)}$.

3) Prescribed-time control: To obtain the prescribed-time convergence property, a time-varying scaling function is defined as [47]

$$\mu(t)=\begin{cases}\frac{T^b}{(T+t_0-t)^b}, & t_0\le t<t_1\\ 1, & t_1\le t\end{cases} \tag{2}$$

where $b\ge 2$ and $t_1=t_0+T$ are any user-set constants. Note that $\mu(t)^{-\varkappa}(\varkappa\in\Re^+)$ is monotonically decreasing for $t\in[t_0,t_1)$, $\mu(t_0)^{-\varkappa}=1$ and $\lim_{t\mapsto t_1^-}\mu(t)^{-\varkappa}=0$. Besides, one has $\dot{\mu}(t)=b/T\mu^{1+1/b}$ for $t\in[t_0,t_1)$ and $\dot{\mu}(t)=0$ for $t\in[t_1,\infty)$.

Lemma 1 ([47]): Consider a system $\dot{x}(t)=f(x(t),t)$, $t\in\Re^+$, $x_0=x(t_0)$. Construct a continuously differentiable function $V(x(t),t):U\times\Re^+\mapsto\Re$ with $U\subset\Re^m$ being a

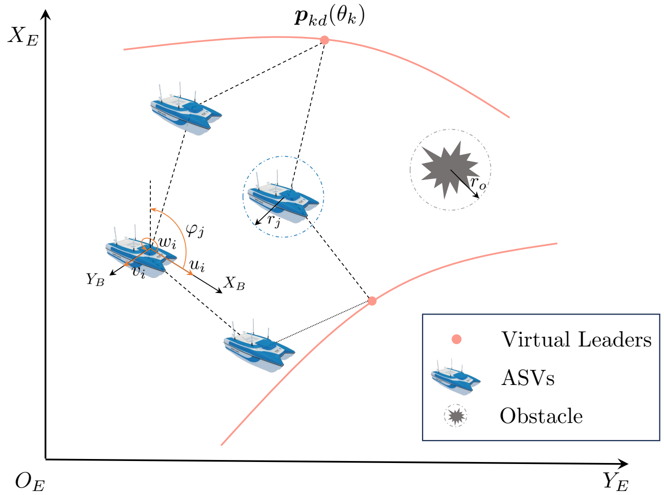

Fig. 1: An illustration for safe cooperative maneuvering of a group of ASVs in an obstacle-loaded environment.

domain including the origin. If there exists a constant $k \in \Re^+$ such that $V(0,t) = 0$, $V(x(t),t) > 0$ in $U - \{0\}$, and $\dot{V} = -kV - 2\dot{\mu}/\mu V$ in U on $[t_0,\infty)$, then the origin of system $\dot{x}(t) = f(x(t),t)$ is prescribed-time stable. It holds $V(t) \le \mu^{-2}\mathrm{e}^{-k(t-t_0)}V(t_0)$ for $t \in [t_0,t_1)$, and $V(t) \equiv 0$ for $t \in [t_1,\infty)$.

B. Problem formulation

As shown in Fig. 1, two reference frames, earth-fixed and body-fixed reference frames, are employed to describe the horizontal motion of M ASVs. For underactuated ASVs, it usually ignores the heave, pitch, and roll due to the X_B-Z_B-plane symmetry [48]. Then, the model dynamics of ith ASV is expressed as below

$$\begin{cases} \dot{p}_i = \mathcal{R}(\varphi_i)\nu_i \\ \dot{\varphi}_i = w_i \\ \dot{u}_i = \dfrac{m_{iv}}{m_{iu}}v_i w_i - \dfrac{d_{iu}}{m_{iu}}u_i + \dfrac{1}{m_{iu}}(\tau_{iu} + \tau_{iu}^d) \\ \dot{v}_i = -\dfrac{m_{iu}}{m_{iv}}u_i w_i - \dfrac{d_{iv}}{m_{iv}}v_i + \dfrac{1}{m_{iv}}\tau_{iv}^d \\ \dot{w}_i = \dfrac{m_{iu} - m_{iv}}{m_{iw}}u_i v_i - \dfrac{d_{iw}}{m_{iw}}w_i + \dfrac{1}{m_{iw}}(\tau_{iw} + \tau_{iw}^d) \end{cases} \tag{3}$$

where $i = 1,\cdots,M$; $p_i = [x_i, y_i]^T$ and φ_i denote the position and yaw angle; $\nu_i = [u_i, v_i]^T$ and w_i represent the velocity information in the surge, sway, and yaw axes; m_{iu}, m_{iv}, and m_{iw} are the masses and inertia, respectively; d_{iu}, d_{iv}, and d_{iw} are the damping parameters; τ_{iu} and τ_{iw} stand for the surge force and yaw moment, respectively; τ_{iu}^d, τ_{iv}^d, and τ_{iw}^d denote the external disturbances; $\mathcal{R}(\varphi_i)$ is a rotation matrix with the following property.

Proposition 1 ([28]): The rotation matrix $\mathcal{R}_i$ is orthogonal satisfying $\|\mathcal{R}_i\| = 1$, $\mathcal{R}_i^{-1} = \mathcal{R}_i^T$, and $\dot{\mathcal{R}}_i = w_i S \mathcal{R}_i$ with

$$\mathcal{R}_i = \begin{bmatrix} \cos\varphi_i & -\sin\varphi_i \\ \sin\varphi_i & \cos\varphi_i \end{bmatrix} \text{ and } S = \begin{bmatrix} 0 & -1 \\ 1 & 0 \end{bmatrix}.$$

Assume that there exist $N_o \ge 0$ obstacles modeled as a Euclidean plane zone $\mathcal{O}_o \in \Re^2$ with the center $p_o \in \Re^2$, $o = 1,...,N_o$. The boundary of zone $\mathcal{O}_o$ is denoted by $\partial\mathcal{O}_o \in \Re^2$. In this paper, the obstacle is assumed as to be circular with $\partial\mathcal{O}_o = \{p \in \Re^2 \mid \|p - p_o\|^2 - r_o^2 = 0\}$, where $r_o \in \Re^+$ represents the radius of the oth circular obstacle.

Definition 1 (Obstacle avoidance zone): For an open set $\mathcal{C}_{io}(p_i) = \{p_i \in \Re^2 \mid \|p_i - p_o\|^2 < (r_o + R_\mathrm{obs})^2\}$ with $R_\mathrm{obs} > 0$ being a user-specified constant, the obstacle avoidance zone $\mathcal{C}_i(p_i)$ is defined by $\mathcal{C}_i(p_i) = \bigcup_{o=1}^{N_o}\mathcal{C}_{io}(p_i)$.

Aside from avoiding obstacles, each ASV must also ensure a safe distance from other ASVs to avoid collisions. Similar to obstacles, each ASV can be enclosed by a circular zone with a center p_i and a radius r_i, $i = 1,...,M$. Then, the ASV avoidance zone for the ith ASV is defined as follows.

Definition 2 (ASV avoidance zone): For an open set $\mathcal{S}_{ij}(p_i) = \{p_i \in \Re^2 \mid \|p_i - p_j\|^2 < (r_i + r_j + R_\mathrm{veh})^2\}$, $j = 1,...,M$, $j \ne i$ with $R_\mathrm{veh} > 0$ being a user-specified constant, the ASV avoidance zone $\mathcal{S}_i(p_i)$ is defined by $\mathcal{S}_i(p_i) = \bigcup_{j=1,\ j\ne i}^{M}\mathcal{S}_{ij}(p_i)$.

Remark 1: Even if an obstacle or an ASV is not circular, possibly even having nonsmooth edges, a circle with the smallest radius enables the obstacle or ASV to be enclosed. Although the larger R_obs and R_veh are to be desired for safety purposes, the overlarge values may lead to some unnecessary sacrifices in cooperative performance. Then, the selection of these parameters is recommended to hold a trade-off between safety and stability. The collision-free protocol designs based on circular obstacles have been widely used in multi-robot systems [34], [49], [50].

In order to achieve cooperative behavior of M ASVs guided by $(N - M)$ virtual leaders, a series of parameterized paths are first defined as follows

$$p_{kd}(\theta_k) = [x_{kd}(\theta_k), y_{kd}(\theta_k)]^T \in \Re^2 \tag{4}$$

where $k = M+1,\cdots,N$; $\theta_k \in [0,1)$ is a path variable. Suppose that $p_{kr}(\theta_k)$ and its partial derivative $p_{kr}^{\theta_k} = \partial p_{kr}(\theta_k)/\partial\theta_k$ are bounded. Some necessary assumptions are given as follows.

Assumption 1 ([14]): The graph $\mathcal{G}$ is undirected and has a spanning tree with the super leader being a root node.

Assumption 2 ([43]): The external disturbances for each ASV are bounded, i.e., $\|\tau_i^d\| \le \bar{\tau}_i^d \in \Re^+$ with $\tau_i^d = [\tau_{iu}^d, \tau_{iv}^d, \tau_{iw}^d]^T$.

For practical ASV systems, external disturbances are caused by winds, waves, and currents with the limited energy. Thus, Assumption 2 is reasonable.

In an obstacle-loaded environment, all ASVs not only execute the graph-defined cooperative pattern but also ensure the their own safety. In what follows, this paper aims to develop a performance-prescribed collision-free cooperative maneuvering method for underactuated ASVs such that:

1) Cooperation objectives:

- *Geometric Objective:* Conduct each ASV to converge to a convex hull spanned by virtual leaders, i.e.

$$\left\| p_i - \sum_{k=M+1}^{N} \beta_{ki} p_{kd}(\theta_k) \right\| \leq \varepsilon_{ip} \in \Re^+ \tag{5}$$

where $\beta_{ki} \in \Re^+$ is a constant with $\sum_{k=M+1}^{N} \beta_{ki} = 1$.

- *Dynamic objective:* Force each virtual leader to complete the velocity task and phase task, i.e.

$$\begin{aligned} &\text{Velocity task:} \quad |\dot{\theta}_k - \upsilon_s| \leq \varepsilon_{k\theta 1} \in \Re^+ \\ &\text{Phase task:} \quad |\theta_k - \theta_0 - \mathcal{P}_k| \leq \varepsilon_{k\theta 2} \in \Re^+ \end{aligned} \tag{6}$$

where $k = M+1, ..., N$; $\upsilon_s \in \Re$ denotes the update velocity of path variable θ_0 for super leader with $\dot{\theta}_0 = \upsilon_s$; $\mathcal{P}_k \in \Re$ is a user-predefined deviation.

2) Safety objectives:

- *Avoidance collision:* Hold each ASV away from ASV avoidance zone, i.e.

$$p_i \notin \mathcal{S}_{ij}(p_i), \ j = 1, ..., M, \ j \neq i, \ \forall t \geq t_0. \tag{7}$$

- *Avoidance obstacles:* Keep each ASV away from the obstacle avoidance zone, i.e.

$$p_i \notin \mathcal{C}_{io}(p_i), \ o = 1, ..., N_o, \ \forall t \geq t_0. \tag{8}$$

III. Constrained Safe Controller Design

In this section, we present a constrained safe cooperative maneuvering method for underactuated ASVs by developing performance-prescribed guidance laws, a barrier-certified yaw velocity protocol, and PTDO-based control laws.

A. Performance-Prescribed Guidance Laws

To achieve the cooperative maneuvering guided by multiple virtual leaders, a distributed error $p_{ie} = [x_{ie}, y_{ie}]^T$ for the ith ASV is defined as

$$p_{ie} = \sum_{j \in \mathcal{N}_i^F} a_{ij}(p_i - p_j) + \sum_{k \in \mathcal{N}_i^L} a_{ik}(p_i - p_{kd}(\theta_k)). \tag{9}$$

With the error vector p_{ie}, a guidance heading angle $\varphi_{id} \in (-\pi, \pi]$ is obtained by

$$\varphi_{id} = \operatorname{atan2}(y_{ie}, x_{ie}) - \pi \operatorname{sign}(y_{ie}) \tag{10}$$

where $\operatorname{atan2}(\cdot,\cdot) \in (-\pi, \pi]$ is an inverse tangent function.

Then, the relative distance z_{i1} and the heading error z_{i2} are presented as follows

$$\begin{cases} z_{i1} = \|p_{ie}\| \\ z_{i2} = \varphi_i - \varphi_{id}. \end{cases} \tag{11}$$

In order to allow users to preset performance indices of cooperative maneuvering, we propose the avoidance-tolerant prescribed performance (ATPP) to force errors z_{i1} and z_{i2} with respect to

$$-z_{ib}^l - \lambda_{ib}^l \leq z_{ib} \leq z_{ib}^r + \lambda_{ib}^r, \ b = 1, 2 \tag{12}$$

with

$$\begin{aligned} z_{ib}^r &= [\delta_{ib}^r + \operatorname{sign}(z_{ib}(t_0))]\rho_{ib} - \rho_{i\infty} \operatorname{sign}(z_{ib}(t_0)) \\ z_{ib}^l &= [\delta_{ib}^l - \operatorname{sign}(z_{ib}(t_0))]\rho_{ib} + \rho_{i\infty} \operatorname{sign}(z(_{ib}t_0)) \end{aligned} \tag{13}$$

where $0 \leq \delta_{ib}^r, \delta_{ib}^l \leq 1$ are scale parameters; $\rho_{ib}(t)$ is a monotonically decreasing function defined as $\rho_{ib} = (\rho_{ib,0} - \rho_{ib,\infty})e^{-\iota_{ib}(t-t_0)} + \rho_{ib,\infty}$ with $\rho_{ib,0} = \rho_{ib}(t_0)$, $\rho_{ib,\infty} = \lim_{t\to\infty} \rho_{ib}(t)$, $\rho_{ib,0} > \rho_{ib,\infty} > 0$, and $\iota_{ib} > 0$; $\lambda_{ib}^r \geq 0$ and $\lambda_{ib}^l \geq 0$ are non-negative adjusted variables to eliminate the limitation of inflexible bounds. Note that the initial errors $z_{i1}(t_0)$ and $z_{i2}(t_0)$ satisfy the ATPP constraints, i.e., $0 < z_{i1}(t_0) < z_{i1}^r(t_0)$ and $-z_{i2}^r(t_0) < z_{i2}(t_0) < z_{i2}^r(t_0)$ for $p_i(t_0) \notin \mathcal{C}_i(p_i) \bigcup \mathcal{S}_i(p_i)$ with $i \in \mathcal{V}^F$.

Based on the PPC methodology [19], a nonlinear mapping from original error z_{ib} to transformed variable ξ_{ib} is formulated as below

$$z_{ib} = 0.5(\bar{z}_{ib}^r + \underline{z}_{ib}^l)\Upsilon(\xi_{ib}) + 0.5(\bar{z}_{ib}^r - \underline{z}_{ib}^l) \tag{14}$$

where $\bar{z}_{ib}^r = z_{ib}^r + \lambda_{ib}^r$ and $\underline{z}_{ib}^l = z_{ib}^l + \lambda_{ib}^l$; $\Upsilon(\xi_{ib}) : (-\infty, \infty) \mapsto [-1, 1]$ is a smooth and monotonically increasing function.

With the error transformation function $\Upsilon(\xi_{ib}) = 2/\pi \arctan(\xi_{ib})$, the corresponding unconstrained variables ξ_{ib} for z_{ib} is yielded by (14),

$$\xi_{ib} = \Upsilon^{-1}\left(z_{ib}, \bar{z}_{ib}^r, \underline{z}_{ib}^l\right) = \tan\left(\frac{\pi}{2} \frac{2z_{ib} - \bar{z}_{ib}^r + \underline{z}_{ib}^l}{\bar{z}_{ib}^r + \underline{z}_{ib}^l}\right). \tag{15}$$

Let $\mathcal{F}_{ib} = \partial\xi_{ib}/\partial z_{ib}$, $\mathcal{F}_{ib}^r = \partial\xi_{ib}/\partial\bar{z}_{ib}^r$, and $\mathcal{F}_{ib}^l = \partial\xi_{ib}/\partial\underline{z}_{ib}^l$, and take the derivative of ξ_{ib} along (15) as

$$\dot{\xi}_{ib} = \mathcal{F}_{ib}\dot{z}_{ib} + \mathcal{F}_{ib}^r(\dot{z}_{ib}^r + \dot{\lambda}_{ib}^r) + \mathcal{F}_{ib}^l(\dot{z}_{ib}^l + \dot{\lambda}_{ib}^l). \tag{16}$$

Since $p_{ie}/\|p_{ie}\| = [\cos(\varphi_{id} + \pi \operatorname{sign}(y_{ie})), \sin(\varphi_{id} + \pi \operatorname{sign}(y_{ie}))]^T = [-\cos(\varphi_{id}), -\sin(\varphi_{id})]^T$ and $\cos(z_{i2}) = 1 - 2\sin^2(z_{i2}/2)$, the derivatives of z_{i1} and z_{i2} are taken as

$$\begin{cases} \dot{z}_{i1} = -d_i\Big[u_i - 2u_i\sin^2\left(\dfrac{z_{i2}}{2}\right) - v_i\sin(z_{i2})\Big] \\ \qquad - \dfrac{p_{ie}^T}{\|p_{ie}\|}\Big[\displaystyle\sum_{j\in\mathcal{N}_i^F} a_{ij}\mathcal{R}_j\nu_j + \sum_{k\in\mathcal{N}_i^L} a_{ik}p_{kd}^{\theta_k}\upsilon_s \\ \qquad - \displaystyle\sum_{k\in\mathcal{N}_i^L} a_{ik}p_{kd}^{\theta_k}\varpi_k\Big] \\ \dot{z}_{i2} = w_i - \dot{\varphi}_{id} \end{cases} \tag{17}$$

where $d_i = \sum_{j\in\mathcal{N}_i^F} a_{ij} + \sum_{k\in\mathcal{N}_i^L} a_{ik}$.

In what follows, we design a first-order auxiliary system to update variables λ_{ib}^r and λ_{ib}^l. Considering the unknown direction of error changes caused by collision avoidance, the auxiliary system is constructed as follows

$$\begin{cases} \dot{\lambda}_{ib}^r = -\mathcal{F}_{ib}/\mathcal{F}_{ib}^r(-\kappa_{ib}\lambda_{ib}^r + G_{ib}^r), & \lambda_{ib}^r(t_0) = 0 \\ \dot{\lambda}_{ib}^l = \mathcal{F}_{ib}/\mathcal{F}_{ib}^l(-\kappa_{ib}\lambda_{ib}^l + G_{ib}^l), & \lambda_{ib}^l(t_0) = 0 \end{cases} \tag{18}$$

where κ is a positive constant; $G_{ib}^r(z_{ib}) = G_{ib}^l(z_{ib}) = \bigvee_{j=1,...,M, j\neq i, o=1,...,N_o}[\|p_i - p_o\| - (r_o + R_{\text{obs}}) < 0 \bigvee \|p_i - p_j\| - (r_i + r_j + R_{\text{veh}}) < 0]\Pi_{ib}\sin(\pi/2 * |z_{ib}|/\Pi_{ib})$.

To drive errors z_{i1} and z_{i2} to converge under constraints (12), the surge and yaw guidance velocities α_{iu} and α_{iw} with (16), (17), and (18), are presented as follows

$$\begin{aligned}\alpha_{iu} =& \frac{1}{d_i}\Big\{\frac{1}{\mathcal{F}_{i1}}(k_{iu}^g\xi_{i1}+\mathcal{F}_{i1}^r\dot{z}_{i1}^r)+\kappa_{i1}(\lambda_{i1}^r-\lambda_{i1}^l)\\ &-\frac{p_{ie}^T}{\|p_{ie}\|}\Big[\sum_{j\in\mathcal{N}_i^F}a_{ij}\mathcal{R}_j\nu_j+\sum_{k\in\mathcal{N}_i^L}a_{ik}p_{kd}^{\theta_k}v_s\Big]\\ &+2u_i\sin^2\left(\frac{z_{i2}}{2}\right)+v_i\sin(z_{i2})\Big\}\end{aligned} \tag{19}$$

$$\begin{aligned}\alpha_{iw} =& -\frac{1}{\mathcal{F}_{i2}}\left(k_{iw}^g\xi_{i2}+\mathcal{F}_{i2}^r\dot{z}_{i2}^r+\mathcal{F}_{i2}^l\dot{z}_{i2}^l\right)+\dot{\psi}_{id}\\ &+\kappa_{i2}\left(\lambda_{i2}^r-\lambda_{i2}^l\right)\end{aligned} \tag{20}$$

where k_{iu}^g, $k_{iw}^g \in \Re^+$. Note that it always holds $z_{i1} \geq 0$ by the definition of the relative distance in (11). Thus, z_{i1}^l is set to zero, and one has $\dot{z}_{i1}^l = 0$.

To coordinate with ASVs and virtual leaders, the path variable θ_k for the kth virtual leader is updated by

$$\dot{\theta}_k = v_s - \varpi_k = v_s + \iota_k\phi_k, \tag{21}$$

where $\iota_k \in \Re^+$ is a constant; $\phi_k = \phi_{k1} - \phi_{k2}$ with

$$\begin{cases}\phi_{k1} = \sum_{i\in\mathcal{N}_k^F}a_{ki}\mathcal{F}_{i1}\frac{p_{ie}^T}{\|p_{ie}\|}p_{kd}^{\theta_k}\xi_{i1}\\ \phi_{k2} = \sum_{l\in\mathcal{N}_k^L}a_{kl}\theta_{kl}+a_{k0}\theta_{ke}\end{cases} \tag{22}$$

where $\theta_{kl} = \theta_k - \theta_l - \mathcal{P}_{kl}$ and $\theta_{ke} = \theta_k - \theta_0 - \mathcal{P}_k$ with $\mathcal{P}_{kl} = \mathcal{P}_k - \mathcal{P}_l$ represent the coordination errors between virtual leaders and between virtual leaders and the super leader, respectively.

Combining (19), (20), (22) with (18), (17), (16), and (21), the kinematic error dynamics can be given by

$$\begin{cases}\dot{\xi}_{i1} = -k_{iu}^g\xi_{i1}-\mathcal{F}_{i1}\left(d_iu_{ie}-\frac{p_{ie}^T}{\|p_{ie}\|}\sum_{k\in\mathcal{N}_i^L}a_{ik}p_{kd}^{\theta_k}\varpi_k\right)\\ \dot{\xi}_{i2} = -k_{iw}^g\xi_{i2}+\mathcal{F}_{i2}w_{ie}\\ \dot{\theta}_{ke} = -\varpi_k\end{cases} \tag{23}$$

where $u_{ie} = u_i - \alpha_{iu}$ and $w_{ie} = w_i - \alpha_{iw}$.

B. PTDO-Based Antidisturbance Control Laws

For underactuated ASVs, we only consider its surge and yaw dynamics expressed as below:

$$\begin{cases}\dot{u}_i = \sigma_{iu}(u_i,v_i,w_i)+\frac{1}{m_{iu}}(\tau_{iu}^d+\tau_{iu})\\ \dot{w}_i = \sigma_{iw}(u_i,v_i,w_i)+\frac{1}{m_{iw}}(\tau_{iw}^d+\tau_{iw})\end{cases} \tag{24}$$

where $\sigma_{iu}(u_i,v_i,w_i) = (m_{iv}v_iw_i - d_{iu}u_i)/m_{iu}$ and $\sigma_{iw}(u_i,v_i,w_i) = [(m_{iu}-m_{iv})u_iv_i - d_{iw}w_i]/m_{iw}$ are available functions.

Based on the simplified model (24), two auxiliary variables $\zeta_{iu} \in \Re$ and $\zeta_{iw} \in \Re$ are introduced to construct the reduced-order disturbance observer. To improve the estimation performance for external disturbances τ_{iu}^d and τ_{iw}^d, the following PTDOs with (2) are developed as follows

$$\begin{cases}\hat{\tau}_{iu}^d = k_{iu}^{1o}\Gamma_{iu}+k_{iu}^{2o}\frac{\Gamma_{iu}}{|\Gamma_{iu}|+\Delta_{iu}}+k_{iu}^{3o}\frac{\dot{\mu}}{\mu}\Gamma_{iu}\\ \dot{\zeta}_{iu} = \sigma_{iu}(u_i,v_i,w_i)+\frac{1}{m_{iu}}(\hat{\tau}_{iu}^d+\tau_{iu})\\ \hat{\tau}_{iw}^d = k_{iw}^{1o}\Gamma_{iw}+k_{iw}^{2o}\frac{\Gamma_{iw}}{|\Gamma_{iw}|+\Delta_{iw}}+k_{iw}^{3o}\frac{\dot{\mu}}{\mu}\Gamma_{iw}\\ \dot{\zeta}_{iw} = \sigma_{iw}(u_i,v_i,w_i)+\frac{1}{m_{iw}}(\hat{\tau}_{iw}^d+\tau_{iw})\end{cases} \tag{25}$$

where $\hat{\tau}_{iu}^d \in \Re$ and $\hat{\tau}_{iw}^d \in \Re$ represent the estimation values of τ_{iu}^d and τ_{iw}^d, respectively; $\Gamma_{iu} = u_i - \zeta_{iu}$ and $\Gamma_{iw} = w_i - \zeta_{iw}$; $k_{iu}^{1o} \in \Re^+$, $k_{iu}^{2o} \in \Re^+$, $k_{iu}^{3o} \in \Re^+$, $k_{iw}^{1o} \in \Re^+$, $k_{iw}^{2o} \in \Re^+$, and $k_{iw}^{3o} \in \Re^+$ are observer gains; $\Delta_{iu} \in \Re^+$ and $\Delta_{iw} \in \Re^+$ are small scalars.

Define $z_{i3} = u_{ie}$ and $z_{i4} = w_i - \alpha_{iw}^*$ and take the derivatives of z_{i3} and z_{i4} along (24) as

$$\begin{cases}\dot{z}_{i3} = \sigma_{iu}(u_i,v_i,w_i)+\frac{1}{m_{iu}}(\tau_{iu}^d+\tau_{iu})-\dot{\alpha}_{iu}\\ \dot{z}_{i4} = \sigma_{iw}(u_i,v_i,w_i)+\frac{1}{m_{iw}}(\tau_{iw}^d+\tau_{iw})-\dot{\alpha}_{iw}^*.\end{cases} \tag{26}$$

With antidisturbance rejection control technique, the surge and yaw control laws based on PTDOs (25) are devised as

$$\begin{cases}\tau_{iu} = m_{iu}[-k_{iu}^cz_{i3}-\sigma_{iu}(u_i,v_i,w_i)+\dot{\alpha}_{iu}]-\hat{\tau}_{iu}^d\\ \tau_{iw} = m_{iw}[-k_{iw}^cz_{i4}-\sigma_{iw}(u_i,v_i,w_i)+\dot{\alpha}_{iw}^*]-\hat{\tau}_{iw}^d\end{cases} \tag{27}$$

where $k_{iu}^c \in \Re^+$ and $k_{iw}^c \in \Re^+$ are control gain constants.

Substituting (27) into (26), the kinetic error dynamics are presented as

$$\begin{cases}\dot{z}_{i3} = -k_{iu}^cz_{i3}+\frac{1}{m_{iu}}\tilde{\tau}_{iu}^d\\ \dot{z}_{i4} = -k_{iw}^cz_{i4}+\frac{1}{m_{iw}}\tilde{\tau}_{iw}^d\end{cases} \tag{28}$$

with $\tilde{\tau}_{iu}^d = \tau_{iu}^d - \hat{\tau}_{iu}^d$ and $\tilde{\tau}_{iw}^d = \tau_{iw}^d - \hat{\tau}_{iw}^d$.

C. The barrier-certified yaw velocity protocol

In the previous subsection, performance-prescribed surge and yaw guidance laws have been developed for underactuated ASVs. The proposed guidance laws (19) and (20) are viewed as nominal guidance laws for stabilizing the relative distance and heading errors, which cannot ensure the safety of multi-ASV system. Thus, this part will present a barrier-certified yaw velocity protocol to modify the nominal guidance laws for the safety of multi-ASV system.

Before designing the barrier-certified yaw velocity protocol, rewrite the kinematic dynamics of ASVs as follows

$$\begin{bmatrix}\dot{p}_i\\ \dot{\varphi}_i\end{bmatrix} = \underbrace{\begin{bmatrix}\mathcal{R}_i(\varphi_i)\nu_i\\ 0\end{bmatrix}}_{f_i}+\underbrace{\begin{bmatrix}0_2\\ 1\end{bmatrix}}_{g_i}\times w_i. \tag{29}$$

In order to ensure no collision with the oth obstacle, the ith ASV is forced to leave obstacle avoidance zone described by

Definition 1, i.e. $p_i \notin \mathcal{C}_{io}(p_i)$ for $\forall t \geq t_0$. Motivated by the set invariance [51], a set $\bar{\mathcal{C}}_{io}(p_i)$ for the ith ASV is defined below

$$\bar{\mathcal{C}}_{io}(p_i) = \{p_i \in \Re^2 \mid h_{io}(p_i) \geq 0\} \tag{30}$$

where $\bar{\mathcal{C}}_{io}(p_i)$ is regarded as a complement of $\mathcal{C}_{io}(p_i)$; $h_{io}(p_i) = \|p_i - p_o\|^2 - (r_o + R_{\text{obs}})^2$ is a control barrier function.

Because the first-order derivative of h_{io} along system (29) does not contain the velocity signal w_i, h_{io} is regarded as a second-order CBF for system (29) by the definition of relative degree [51]. Next, the following sets $\bar{\mathcal{C}}_{io,1}(p_i)$, and $\bar{\mathcal{C}}_{io,2}(p_i)$ are presented as

$$\begin{aligned} \bar{\mathcal{C}}_{io,1}(p_i) &= \{p_i \in \Re^2 \mid \chi_{io,0}(p_i) \geq 0\} \\ \bar{\mathcal{C}}_{io,2}(p_i) &= \{p_i \in \Re^2 \mid \chi_{io,1}(p_i) \geq 0\} \end{aligned} \tag{31}$$

where $\chi_{io,0}$ and $\chi_{io,1}$ are the differentiable functions expressed by $\chi_{io,0}(p_i) = h_{io}(p_i)$ and $\chi_{io,1}(p_i) = \dot{\chi}_{io,0}(p_i) + \beta_{io,1}\chi_{io,0}(p_i)$ with $\beta_{io,1} \in \Re^+$. Then, the forward invariance of $\bar{\mathcal{C}}_{io,1}(p_i)$ can be guaranteed if the set $\bar{\mathcal{C}}_{io,1}(p_i) \cap \bar{\mathcal{C}}_{io,2}(p_i)$ is forward invariant [51].

To ensure the forward invariance of the set $\bar{\mathcal{C}}_{io,1}(p_i) \cap \bar{\mathcal{C}}_{io,2}(p_i)$, an obstacle-avoided yaw velocity constraint is yielded as

$$\begin{aligned} \mathcal{W}_{io} = \Big\{ w_i \in \Re \mid\ & L^2_{f_i} h_{io} + L_{g_i} L_{f_i} h_{io} w_i \\ & + O_{io}(h_{io}) + \beta_{io,2}\chi_{io,1} \geq 0 \Big\} \end{aligned} \tag{32}$$

where $\beta_{io,2} \in \Re^+$; $L^2_{f_i} h_{io}$ and $L_{g_i} L_{f_i} h_{io}$ are Lie derivatives for system (29); $O_{io}(h_{io})$ denotes the remaining Lie derivatives with the relative degree 0 or 1.

According to Definition 2, a set $\bar{\mathcal{S}}_{ij}(p_i)$, viewed as a complement of $\mathcal{S}_{ij}(p_i)$, is defined to describe the safety objective among ASVs as follows

$$\bar{\mathcal{S}}_{ij}(p_i) = \{p_i \in \Re^2 \mid h_{ij}(p_i) \geq 0\} \tag{33}$$

with $h_{ij}(p_i) = \|p_i - p_j\|^2 - (r_i + r_j + R_{\text{veh}})^2$. Similar to (31), two sets associated with $\bar{\mathcal{S}}_{ij}(p_i)$ are presented as

$$\begin{aligned} \bar{\mathcal{S}}_{ij,1}(p_i) &= \{p_i \in \Re^2 \mid \chi_{ij,0}(p_i) \geq 0\} \\ \bar{\mathcal{S}}_{ij,2}(p_i) &= \{p_i \in \Re^2 \mid \chi_{ij,1}(p_i) \geq 0\} \end{aligned} \tag{34}$$

where $\chi_{ij,0}(p_i) = h_{ij}(p_i)$ and $\chi_{ij,1}(p_i) = \dot{\chi}_{ij,0}(p_i) + \beta_{ij,1}\chi_{ij,0}(p_i)$ with $\beta_{ij,1} \in \Re^+$.

Then, an ASV-avoided yaw velocity constraint is given by

$$\begin{aligned} \mathcal{W}_{ij} = \Big\{ w_i \in \Re \mid\ & L^2_{f_i} h_{ij} + L_{g_i} L_{f_i} h_{ij} w_i \\ & + O_{ij}(h_{ij}) + \beta_{ij,2}\chi_{ij,1} \geq 0 \Big\} \end{aligned} \tag{35}$$

where $\beta_{ij,2} \in \Re^+$; $L^2_{f_i} h_{ij}$ and $L_{g_i} L_{f_i} h_{ij}$ are Lie derivatives; $O_{ij}(h_{ij})$ is also the remaining Lie derivative.

The barrier-certified yaw velocity for the safety of the ith ASV must satisfy the constraint $\mathcal{U}_{io} \cap \mathcal{U}_{ij}$, $o \in \{1, ..., N_o\}, j \in \{1, ..., M\} \setminus \{i\}$. Thus, a barrier-certified yaw velocity protocol is formulated by the following quadratic optimization

$$\begin{aligned} \alpha^*_{iw} =& \arg \min_{w_i \in \Re} \ J(w_i) = \|w_i - \alpha_{iw}\|^2 \\ \text{s.t.} \quad & w_i \in \mathcal{W}_{io} \cap \mathcal{W}_{ij},\ o \in \{1, ..., N_o\}, j \in \mathcal{V}^F \setminus \{i\} \end{aligned} \tag{36}$$

where α^*_{iw} is the optimal yaw velocity for stability and safety.

To facilitate the implementation of the optimization problem (36), an online optimization technique is employed by a recurrent neural network (RNN)

$$\dot{w}_i = -\frac{1}{\epsilon_i}\Big[\nabla J(w_i) + \varsigma_i \sum_{l=1}^{M+N_o-1} \partial \max\{0, \Xi_{il}(w_i)\}\Big] \tag{37}$$

where $\epsilon_i, \varsigma_i \in \Re^+$; $\Xi_{il}(w_i) = -L^2_{f_i} h_{ij} - L_{g_i} L_{f_i} h_{ij} w_i - O_{ij}(h_{ij}) - \beta_{ij,2}(h_{ij}), l = 1, ..., M-1$, $\Xi_{il}(w_i) = -L^2_{f_i} h_{io} - L_{g_i} L_{f_i} h_{io} w_i - O_{io}(h_{io}) - \beta_{io,2}(h_{io}), l = M, ..., M + N_o - 1$; $\partial \max\{0, \Xi_{il}(w_i)\}$ represents a piece-wise penalty function defined as

$$\partial \max\{0, \Xi_{il}(w_i)\} = \begin{cases} \nabla \Xi_{il}(w_i), & \Xi_{il}(w_i) > 0 \\ [0, \nabla \Xi_{il}(w_i)], & \Xi_{il}(w_i) = 0 \\ 0, & \Xi_{il}(w_i) < 0. \end{cases}$$

According to [54], the neuronal state w_i of RNN (37) can converge to the optimal solution α^*_{iw} within a finite time.

IV. Main Results

In the previous section, constrained safe cooperative maneuvering method has been proposed for multiple ASVs in an obstacle-loaded environment. The section analyzes the stability and the safety of the closed-loop system.

A. Observation Subsystem

Lemma 2: Under Assumption 2, when $k^{2o}_{iu} \geq \bar{\tau}^d_i$ and $k^{2o}_{iw} \geq \bar{\tau}^d_i$, the disturbance terms τ^d_{iu} and τ^d_{iw} can be precisely estimated by using proposed PTDOs (25) within a prescribed time. Estimation errors $\tilde{\tau}^d_{iu}$ and $\tilde{\tau}^d_{iw}$ are prescribed-time stable.

Proof: Consider a Lyapunov function candidate as

$$V_{i1} = \frac{1}{2}(m_{iu}\Gamma^2_{iu} + m_{iw}\Gamma^2_{iw}). \tag{38}$$

With (24) and (25), it takes the derivative of V_1 as

$$\begin{aligned} \dot{V}_{i1} =& m_{iu}\Gamma_{iu}(\dot{u}_i - \dot{\zeta}_{iu}) + m_{iw}\Gamma_{iw}(\dot{w}_i - \dot{\zeta}_{iw}) \\ =& -\Gamma_{iu}\Big(k^{1o}_{iu}\Gamma_{iu} + k^{2o}_{iu}\frac{\Gamma_{iu}}{|\Gamma_{iu}| + \Delta_{iu}} + k^{3o}_{iu}\frac{\dot{\mu}}{\mu}\Gamma_{iu} - \tau^d_{iu}\Big) \\ & -\Gamma_{iw}\Big(k^{1o}_{iw}\Gamma_{iw} + k^{2o}_{iw}\frac{\Gamma_{iw}}{|\Gamma_{iw}| + \Delta_{iw}} + k^{3o}_{iw}\frac{\dot{\mu}}{\mu}\Gamma_{iw} - \tau^d_{iw}\Big). \end{aligned}$$

Let $\Gamma_i = [\Gamma_{iu}, \Gamma_{iw}]^T$, $K^{1o}_i = \text{diag}\{k^{1o}_{iu}, k^{1o}_{iw}\}$, $K^{2o}_i = \text{diag}\{k^{2o}_{iu}/(|\Gamma_{iu}| + \Delta_{iu}), k^{2o}_{iw}/(|\Gamma_{iw}| + \Delta_{iw})\}$, and $K^{3o}_i = \text{diag}\{k^{3o}_{iu}, k^{3o}_{iw}\}$. Under Assumption 2, we have

$$\begin{aligned} \dot{V}_{i1} \leq & -\underline{\lambda}(K^{1o}_i)\|\Gamma_i\|^2 - \underline{\lambda}(K^{2o}_i)\|\Gamma_i\| \\ & - \underline{\lambda}(K^{3o}_i)\frac{\dot{\mu}}{\mu}\|\Gamma_i\|^2 + \bar{\tau}_{id}\|\Gamma_i\|. \end{aligned} \tag{39}$$

When $\underline{\lambda}(K^{2o}_i) \geq \bar{\tau}_{id}$, it renders that

$$\dot{V}_{i1} \leq -\underline{\lambda}(K^{1o}_i)\|\Gamma_i\|^2 - \underline{\lambda}(K^{3o}_i)\frac{\dot{\mu}}{\mu}\|\Gamma_i\|^2. \tag{40}$$

Since $\underline{\lambda}(K_i^{3o}) \geq \bar{m}_i$ with $\bar{m}_i = \max\{m_{iu}, m_{iw}\}$, it yields from (38) that

$$\begin{aligned}\dot{V}_{i1} \leq & -2\frac{\underline{\lambda}(K_i^{1o})}{\bar{m}_i}V_{i1} - 2\frac{\underline{\lambda}(K_i^{3o})}{\bar{m}_i}\frac{\dot{\mu}}{\mu}V_{i1} \\ \leq & -2\frac{\underline{\lambda}(K_i^{1o})}{\bar{m}_i}V_{i1} - 2\frac{\dot{\mu}}{\mu}V_{i1}.\end{aligned} \tag{41}$$

According to Lemma 1, it obtains

$$V_{i1}(t) \leq \mu^{-2}(t)e^{-2\frac{\underline{\lambda}(K_i^{1o})}{\bar{m}_i}(t-t_0)}V_{i1}(t_0) \tag{42}$$

on $t \in [t_0, T_1)$. It also implies that $\|\Gamma_i(t)\| \leq \mu^{-2}e^{-2\underline{\lambda}(K_i^{1o})(t-t_0)/\bar{m}_i}\|\Gamma_i(t_0)\|$ on $t \in [t_0, T_1)$. Further, it renders that $\lim_{t\mapsto T_1^-}\|\Gamma_i(t)\| \mapsto 0$. Then, we have $\dot{V}_{i1}(t) = 0$ for $t \in [T_1, \infty)$ and $\dot{\Gamma} = 0$ for $t \in [T_1, \infty)$. Using (24) and (25), the estimation error always holds $\tilde{\tau}_i^d = [\tilde{\tau}_{iu}^d, \tilde{\tau}_{iw}^d]^T = \bar{M}_i\Gamma_i$. Hence, it infers that $\tilde{\tau}_i^d = 0$ for $t \in [T_1, \infty)$. □

B. Control Subsystems

Lemma 3: The kinetic subsystem (28) with states z_{i3} and z_{i4} and inputs $\tilde{\tau}_{iu}^d$ and $\tilde{\tau}_{iw}^d$ is input-to-state stable.

Proof: Consider a Lypunov function candidate

$$V_{i2} = \sqrt{\frac{1}{2}(z_{i3}^2 + z_{i4}^2)} \tag{43}$$

and take its derivative along (28) as

$$\begin{aligned}\dot{V}_{i2} = & \frac{1}{2V_{i2}}(z_{i3}\dot{z}_{i3} + z_{i4}\dot{z}_{i4}) \\ = & -\frac{1}{2V_{i2}}(k_{iu}^c z_{i3}^2 + k_{iw}^c z_{i4}^2) \\ & + \frac{1}{2V_{i2}}(\frac{1}{m_{iu}}z_{i3}\tilde{\tau}_{iu}^d + \frac{1}{m_{iw}}z_{i4}\tilde{\tau}_{iw}^d) \\ \leq & -\underline{k}_i^c V_{i2} + \frac{1}{\sqrt{2}\underline{m}_i}\|\tilde{\tau}_i^d\|\end{aligned} \tag{44}$$

where $\underline{k}_i^c = \min\{k_{iu}^c, k_{iw}^c\}$ and $\underline{m}_i = \min\{m_{iu}, m_{iw}\}$. From Lemma 2, $\|\tilde{\tau}_i^d\|$ is bounded such that the kinetic subsystem (28) is input-to-state stable. □

Lemma 4: The kinematic subsystem (23) with states ξ_{i1}, ξ_{i2}, and θ_{ke} and inputs u_{ie} and w_{ie} is input-to-state stable.

Proof: Define vectors $\theta_e = [\theta_{(M+1)e}, ..., \theta_{Ne}]^T$, $\phi_1 = [\phi_{(M+1)1}, ..., \phi_{N1}]^T$, and $\phi_2 = [\phi_{(M+1)2}, ..., \phi_{N2}]^T$. Then, it follows from (22) that

$$\phi_2 = \mathcal{H}\theta_e \tag{45}$$

with $\mathcal{H} = \mathcal{L}_0 + \mathcal{B}_0$, where $\mathcal{B}_0$ is a diagonal matrix with diagonal element being 1 only if the super leader's information is available.

Consider a Lyapunov function candidate V_3 as follows

$$V_3 = \sum_{i=1}^{M}\frac{1}{2}(\xi_{i1}^2 + \xi_{i2}^2) + \frac{1}{2}\theta_e^T\mathcal{H}\theta_e. \tag{46}$$

Using (45), it takes the derivative of V_3 as

$$\dot{V}_3 = \sum_{i=1}^{M}(\xi_{i1}\dot{\xi}_{i1} + \xi_{i2}\dot{\xi}_{i2}) + \sum_{k=M+1}^{N}\phi_{k2}^T\dot{\theta}_{ke}. \tag{47}$$

Along dynamics (22) and (23), it yields that

$$\begin{aligned}\dot{V}_3 = & \sum_{i=1}^{M}\Big(-k_{iu}^g\xi_{i1}^2 - k_{iw}^g\xi_{i2}^2 - d_i\mathcal{F}_{i1}\xi_{i1}u_{ie} + \mathcal{F}_{i2}\xi_{i2}w_{ie} \\ & + \mathcal{F}_{i1}\xi_{i1}\frac{p_{ie}^T}{\|p_{ie}\|}\sum_{k\in\mathcal{N}_i^L}a_{ik}p_{kd}^{\theta_k}\varpi_k\Big) - \sum_{k=M+1}^{N}(\phi_{k1}^T - \phi_k^T)\varpi_k \\ = & \sum_{i=1}^{M}\Big(-k_{iu}^g\xi_{i1}^2 - k_{iw}^g\xi_{i2}^2 - d_i\xi_{i1}\mathcal{F}_{i1}u_{ie} + \xi_{i2}\mathcal{F}_{i2}w_{ie}\Big) \\ & - \sum_{k=M+1}^{N}\iota_k\phi_k^2.\end{aligned} \tag{48}$$

Letting $\xi_i = [\xi_{i1}, \xi_{i2}]^T$ and $\vartheta_{ie} = [u_{ie}, w_{ie}]^T$, it renders from (48) that

$$\begin{aligned}\dot{V}_3 \leq & \sum_{i=1}^{M}\Big(-\underline{\lambda}(K_i^g)\|\xi_i\|^2 + d_i\bar{\lambda}(\mathcal{F}_i)\|\xi_i\|\|\vartheta_{ie}\|\Big) \\ & - \sum_{k=M+1}^{N}\iota_k\phi_k^2.\end{aligned} \tag{49}$$

where $K_i^g = \mathrm{diag}\{k_{iu}^g, k_{iw}^g\}$ and $\mathcal{F}_i = \mathrm{diag}\{\mathcal{F}_{i1}, \mathcal{F}_{i2}\}$.

Define $E' = [\xi^T, \phi^T]^T$ and $E = [\xi^T, \theta_e^T]^T$ with $\xi = [\xi_1^T, ..., \xi_M^T]^T$ and $\phi = [\phi_{M+1}, ..., \phi_N]^T$. According to the fact that $E' = \Lambda E$ where

$$\Lambda = \begin{bmatrix} I_M \otimes I_2 & 0_{2M\times(N-M)} \\ \Psi & -\mathcal{H} \end{bmatrix}$$

$$\Psi = \begin{bmatrix} \Psi_{(M+1)1} & 0 & \cdots & \Psi_{(M+1)M} & 0 \\ \vdots & \vdots & \ddots & \vdots & \vdots \\ \Psi_{N1} & 0 & \cdots & \Psi_{NM} & 0 \end{bmatrix}$$

with $\Psi_{ki} = a_{ki}\mathcal{F}_{i1}p_{ie}^T p_{kd}^{\theta_k}/\|p_{ie}\|$, $i = 1, \ldots, M$, $k = M+1, \ldots, N$, it further follows that

$$\begin{aligned}\dot{V}_3 \leq & -c\|E'\|^2 + \bar{\lambda}_{\mathcal{F}}\|E\|\|d\|\|\vartheta_e\| \\ \leq & -c\underline{\lambda}(\Lambda)\|E\|^2 + \bar{\lambda}_{\mathcal{F}}\|E\|\|d\|\|\vartheta_e\|,\end{aligned} \tag{50}$$

where $c = \min_{i=1,...,M,\ k=M+1,...,N}\{\underline{\lambda}(K_i^g), \iota_k\}$, $\bar{\lambda}_{\mathcal{F}} = \max_{i=1,...,M}\{\bar{\lambda}(\mathcal{F}_i)\}$, $d = \mathrm{diag}\{d_1, 0, ..., d_M, 0\}$, and $\vartheta_e = [\vartheta_{1e}^T, ..., \vartheta_{Me}^T]^T$.

For $\|E\| \geq \bar{\lambda}_{\mathcal{F}}\|d\|\|\vartheta_e\|/(bc\underline{\lambda}(\Lambda))$ with $b \in (0, 1)$, we have

$$\dot{V}_3 \leq -c\underline{\lambda}(\Lambda)(1-b)\|E\|^2. \tag{51}$$

Note that $u_{ie} = z_{i3}$ and $w_{ie} = z_{i4} + \alpha_{iw}^* - \alpha_{iw}$, it gets that u_{ie} and w_{ie} are bounded from Lemma 3. Further, it is deduced that ϑ_e is bounded satisfying $\|\vartheta_e\| \leq \bar{\vartheta}_e \in \Re^+$. Consequently, it concludes that the subsystem (23) is input-to-state stable.□

C. Optimization Subsystem

Lemma 5: For the underactuated ASVs with dynamic (3) and safe velocity constraints (32) and (35), the sets $\bar{\mathcal{C}}_{io}(p_i)$ and $\bar{\mathcal{S}}_{ij}(p_i)$ are guaranteed to be input-to-state safe for $p_i(t_0) \in \bar{\mathcal{C}}_{io}(p_i)$ and $p_i(t_0) \in \bar{\mathcal{S}}_{ij}(p_i)$, i.e. $p_i(t) \in \bar{\mathcal{C}}_{io}(p_i)$ and $p_i(t) \in \bar{\mathcal{S}}_{ij}(p_i)$, $\forall t \geq t_0$.

Proof: Form Lemma 3, it is found that w_i cannot asymptotically converge to α_{iw}^* affected by the bounded disturbance $\tilde{\tau}_{iw}^d$.

Thus, it ensure that $\bar{\mathcal{C}}_{io}(p_i)$ and $\bar{\mathcal{S}}_{ij}(p_i)$ are input-to-state safe in the presence of the bounded disturbance $\tilde{\tau}_{iw}^d$. The slightly larger sets associated with $\tilde{\tau}_{iw}^d$ are defined as below

$$\begin{aligned}
\bar{\mathcal{C}}_{io,1}^d(p_i) &= \{p_i \in \Re^2 \mid \chi_{io,0}(p_i) + \varrho_{io,1}(\|\tilde{\tau}_i^d\|_\infty) \geq 0\} \\
\bar{\mathcal{C}}_{io,2}^d(p_i) &= \{p_i \in \Re^2 \mid \chi_{io,1}(p_i) + \varrho_{io,2}(\|\tilde{\tau}_i^d\|_\infty) \geq 0\} \\
\bar{\mathcal{S}}_{ij,1}^d(p_i) &= \{p_i \in \Re^2 \mid \chi_{ij,0}(p_i) + \varrho_{ij,1}(\|\tilde{\tau}_i^d\|_\infty) \geq 0\} \\
\bar{\mathcal{S}}_{ij,2}^d(p_i) &= \{p_i \in \Re^2 \mid \chi_{ij,1}(p_i) + \varrho_{ij,2}(\|\tilde{\tau}_i^d\|_\infty) \geq 0\}
\end{aligned} \tag{52}$$

where $\varrho_{io,1}(\cdot)$, $\varrho_{io,2}(\cdot)$, $\varrho_{ij,1}(\cdot)$, and $\varrho_{ij,2}(\cdot)$ are class $\mathcal{K}$ functions.

By $\bar{\mathcal{C}}_{io,2}^d(p_i)$ and $\bar{\mathcal{S}}_{ij,2}^d(p_i)$, an extended set is expressed by

$$\Omega_i(p_i) = \{p_i \in \Re^2 \mid \bar{\chi}_{io,1}(p_i) \geq 0, \bar{\chi}_{ij,1}(p_i) \geq 0\} \tag{53}$$

where $\bar{\chi}_{io,1}(p_i) = -V_{i2} + \ell_{io}\chi_{io,1}(p_i) + \ell_{io}\varrho_{io,2}(\|\tilde{\tau}_i^d\|_\infty)$ and $\bar{\chi}_{ij,1}(p_i) = -V_{i2} + \ell_{ij}\chi_{ij,1}(p_i) + \ell_{ij}\varrho_{ij,2}(\|\tilde{\tau}_i^d\|_\infty)$ with $\ell_{io} \in \Re^+$ and $\ell_{ij} \in \Re^+$.

Using $\ell_{i\star}\beta_{i\star,2}\varrho_{i\star,2}(\|\tilde{\tau}_i^d\|_\infty) = \|\tilde{\tau}_i^d\|/\sqrt{2}\underline{m}_i$ with $\star = o, j$, the derivative of $\bar{\chi}_{i\star,1}$ is put into

$$\begin{aligned}
&\dot{\bar{\chi}}_{i\star,1} \\
&= -\dot{V}_{i2} + \ell_{i\star}(L_{f_i}\bar{\chi}_{i\star,1} + L_{g_i}\bar{\chi}_{i\star,1}w_i) \\
&= -\dot{V}_{i2} + \ell_{i\star}(L_{f_i}\bar{\chi}_{i\star,1} + L_{g_i}\bar{\chi}_{i\star,1}(\alpha_{iw}^* + z_{i4})) \\
&\geq \underline{k}_i^c V_{i2} - \frac{1}{\sqrt{2}\underline{m}_i}\|\tilde{\tau}_i^d\| - \ell_{i\star}\beta_{i\star,2}\chi_{i\star,1} - \ell_{i\star}|L_{g_i}\bar{\chi}_{i\star,1}||z_{i4}| \\
&\geq (\underline{k}_i^c - \beta_{i\star,2})V_{i2} - \beta_{i\star,2}\bar{\chi}_{i\star,1} - \ell_{i\star}|L_{g_i}\bar{\chi}_{i\star,1}z_{i4}|
\end{aligned} \tag{54}$$

for $p_i(t_0) \in \Omega_i(p_i)$.

When $\underline{k}_i^c > \beta_{i\star,2}$, it follows that $\dot{\bar{\chi}}_{i\star,1} \geq -\beta_{i\star,2}\bar{\chi}_{i\star,1}$. According to [52], the set $\Omega_i(p_i)$ for $p_i(t_0) \in \Omega_i(p_i)$ is forward invariant, i.e., $p_i(t) \in \Omega_i(p_i), \forall t > t_0$. Obviously, it gets that $\chi_{i\star,1}(p_i) + \varrho_{i\star,2}(\|\tilde{\tau}_i^d\|_\infty) \geq V_{i2}/\ell_{i\star} \geq 0$. Thus, these sets $\bar{\mathcal{C}}_{io,2}^d(p_i)$ and $\bar{\mathcal{S}}_{ij,2}^d(p_i)$ are forward invariant. According to the proof of Lemma 3 in [53], it renders that $\bar{\mathcal{C}}_{io,1}^d(p_i)$ and $\bar{\mathcal{S}}_{ij,1}^d(p_i)$ are also forward invariant, i.e., $\bar{\mathcal{C}}_{io,1}^d(p_i)$ and $\bar{\mathcal{S}}_{ij,1}^d(p_i)$ are safe. Since $\bar{\mathcal{C}}_{io,1}^d(p_i) \supset \bar{\mathcal{C}}_{io,1}(p_i)$ and $\bar{\mathcal{S}}_{ij,1}^d(p_i) \supset \bar{\mathcal{S}}_{ij,1}(p_i)$ from (31), (34) and (52), $\bar{\mathcal{C}}_{io,1}(p_i)$ and $\bar{\mathcal{S}}_{ij,1}(p_i)$ are input-to-state safe. By the fact that $\chi_{io,0} = h_{io}$ and $\chi_{ij,0} = h_{ij}$, it obtains $\bar{\mathcal{C}}_{io,1}(p_i) = \bar{\mathcal{C}}_{io}(p_i)$ and $\bar{\mathcal{S}}_{ij,1}(p_i) = \bar{\mathcal{S}}_{ij}(p_i)$ such that $\bar{\mathcal{C}}_{io}(p_i)$ and $\bar{\mathcal{S}}_{ij}(p_i)$ are input-to-state safe. □

D. Stability and Safety Results

It can be observed from (44) that $\tilde{\tau}_{iu}^d$ and $\tilde{\tau}_{iw}^d$ are inputs of the kinetic subsystem (28). It can be observed from (50) that the states of kinetic subsystem (28) z_{i3} and z_{i4} are some inputs of kinematic subsystem (23). The subsystem (25) and the system cascaded by subsystems (28) and (23) lead to the resulting closed-loop system. Lemmas 2-4 state the stability of all subsystems (23), (25), and (28). Lemma 5 gives the input-to-state safety of multi-ASV system. The stability and safety of the closed-loop system are given via the following theorem.

Theorem 1: Consider a swarm of underactuated ASVs expressed as dynamics (3) with the auxiliary system (18), the kinematic guidance laws (19)-(20), the update law (21), the barrier-certified yaw velocity (37), the PTDOs (25), and the kinetic control laws (27). Under Assumptions 1-2, it is ensured that: 1) all error signals of the closed-loop constrained safe cooperative maneuvering system are bounded; 2) the multi-ASV system is ensured to be input-to-state safe; and 3) the ATPP constraints (12) are not violated.

Proof: From Lemmas 2-4 and Lemma 4.6 in [55], it has concluded that all error signals are bounded. According to definition (9), we have $p_e = \mathcal{L}_1 \otimes I_2[p + (\mathcal{L}_1^{-1}\mathcal{L}_2 \otimes I_2)p_d]$ with $p = [p_1^T, \cdots, p_M^T]^T$ and $p_d = [p_{(M+1)d}^T, \cdots, p_{Nd}^T]^T$. Further, it yields $\|p + (\mathcal{L}_1^{-1}\mathcal{L}_2 \otimes I_2)p_d\| \leq \|p_e\|/\underline{\lambda}(\mathcal{L}_1)$. Under Assumption 1, it gets that the error ξ is bounded by Lemma 4, which means that p_e is bounded by Eq. (11). Then, there exists a positive constant ε_{ip} such that the geometric objective (5) is satisfied. By Lemma 4 and Eq. (22), it yields that θ_e and ϕ_k are bounded. It implies that there exist two positive constants $\varepsilon_{k\theta 1}$ and $\varepsilon_{k\theta 2}$ such that the dynamic objective (6) is achieved. From Lemma 5, it has $p_i(t) \in \bar{\mathcal{C}}_{io}(p_i)$ and $p_i(t) \in \bar{\mathcal{S}}_{ij}(p_i)$, $\forall t \geq t_0$. According to the definitions of $\bar{\mathcal{C}}_{io}(p_i)$ and $\bar{\mathcal{S}}_{ij}(p_i)$, it gets that $p_i(t) \notin \bar{\mathcal{C}}_{io}(p_i)$ and $p_i(t) \notin \bar{\mathcal{S}}_{ij}(p_i)$, $\forall t \geq t_0$, i.e., safety objectives (7)-(8) are achieved. □

V. Simulation Results

This section conducts simulation results to verify the effectiveness of proposed constrained safe cooperative maneuvering method. We consider 3 ASVs (labeled as ASV1, ... , ASV3), 4 virtual leaders, and 1 super leader. A network topology in Fig. 2 is given to formulate the cooperative maneuvering pattern. In addition, three obstacles, i.e., two stationary circular obstacles and one moving ship, are placed to evaluate the ability of collision avoidance.

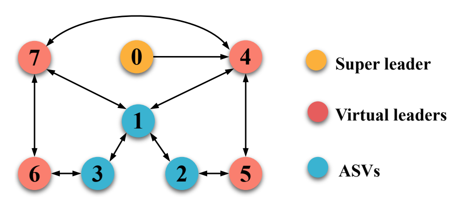

Fig. 2: The network topology.

Suppose that four virtual leaders move along four parametrized paths given as $p_{kd}(\theta_k) = [\frac{\sqrt{2}}{2}v_s\theta_k + \frac{\sqrt{2}}{2}(15\cos(\frac{1}{30}v_s\theta_k + \frac{\pi}{30}) + 40), \frac{\sqrt{2}}{2}v_s\theta_k - \frac{\sqrt{2}}{2}(15\cos(\frac{1}{30}v_s\theta_k + \frac{\pi}{30}) + 40)]^T$ for $k = 4, 5$, $p_{kd}(\theta_k) = [\frac{\sqrt{2}}{2}v_s\theta_k - \frac{\sqrt{2}}{2}(15\cos(\frac{1}{30}v_s\theta_k + \frac{\pi}{30}) + 40), \frac{\sqrt{2}}{2}v_s\theta_k + \frac{\sqrt{2}}{2}(15\cos(\frac{1}{30}v_s\theta_k + \frac{\pi}{30}) + 40)]^T$ for $k = 6, 7$ with $v_s = 0.5$ and $\theta_4(0) = \theta_5(0) = \theta_6(0) = \theta_7(0) = 0$. The deviations of path parameters are set as $\mathcal{P}_4 = \mathcal{P}_7 = 0$ and $\mathcal{P}_5 = -\mathcal{P}_6 = -40$. For the vehicle model, we consider the ASV1∼ASV3 with a length of 1.255 m, and the other Bis-scale parameters: $m_{iu} = 23.8$kg, $m_{iv} = 33.8$kg, $m_{iw} = 2.764$kg, $d_{iu} = 2$, $d_{iv} = 7$, and $d_{iw} = 0.5$. According to Remark 1, the edge-nonsmooth obstacle can be modeled as a circular obstacle. For simplicity, we consider two static circular obstacles (named by Obstacle1 and Obstacle2), and an intersection ASV (named by Obstacle3). The parameters of all ASVs and obstacles are summarized into Table I including the initial

TABLE I: INITIAL VALUES OF ASVS AND OBSTACLES.

i, o = 1,2,3	ASV1	ASV2	ASV3	Obstacle1	Obstacle2	Obstacle3
$[p_i^T(t_0), \varphi_i(t_0)]$ or $p_o^T(t_0)$	$[-2, 0, 0]$	$[15, -20, 0]$	$[-20, 12, 0]$	$[20, 35]$	$[82, 70]$	$[50, 120]$
$[\nu_i^T(t_0), w_i(t_0)]$ or $\dot{p}_o^T(t_0)$	$[0, 0, 0]$	$[0, 0, 0]$	$[0, 0, 0]$	$[0, 0]$	$[0, 0]$	$[0.1, 0]$
r_i or r_o	2	2	2	5	8	2

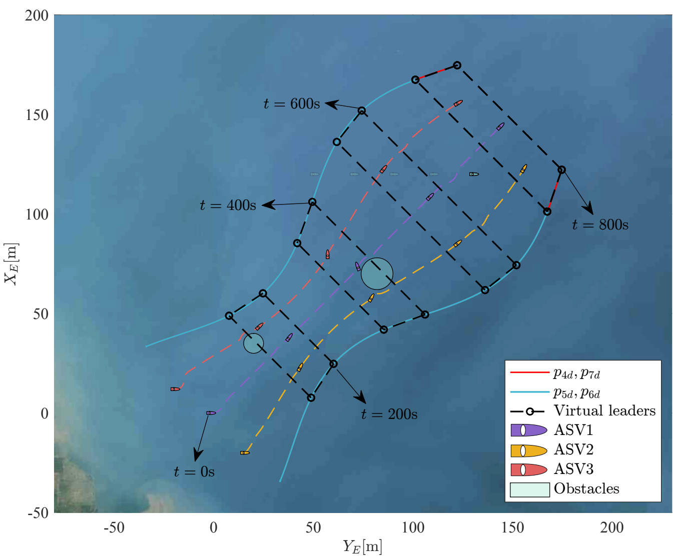

Fig. 3: The constrained safe cooperative maneuvering of 3 underactuated ASVs.

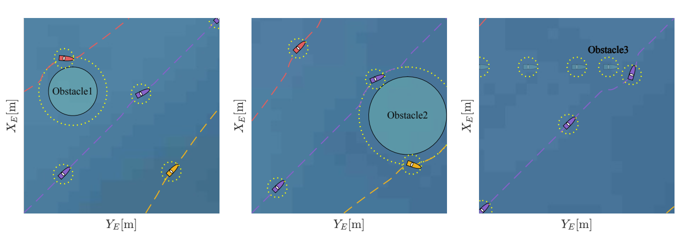

(a) Avoid Obstacle1. (b) Avoid Obstacle2. (c) Avoid Obstacle3.

Fig. 4: The snapshots of collision avoidance for each obstacle.

position, velocity, and radius. To conduct the simulation, the main equations and parameters of presented method are given as below: $\rho_{i1,0} = 10$; $\rho_{i2,0} = 2.0$; $\rho_{i1,\infty} = 1$; $\rho_{i2,\infty} = 0.4$; $\iota_{i1} = 0.05$; $\iota_{i2} = 0.2$; $\delta_{i1}^r = 0.7$; $\delta_{i1}^l = 0.4$; $\delta_{i2}^r = \delta_{i2}^l = 0.5$; $\kappa_{i1} = 0.5$; $\kappa_{i2} = 0.25$; $\Pi_{i1} = 10$; $\Pi_{i2} = \pi$; $k_{iu}^g = 0.5$; $k_{iw}^g = 1.0$; $\iota_k = 0.2$; $\beta_{io,1} = \beta_{io,2} = \beta_{ij,1} = \beta_{ij,2} = 0.5$; $R_{\text{obs}} = 2$; $R_{\text{veh}} = 1$; $\epsilon_i = 1$; $\varsigma_i = 2$; $k_{iu}^{1o} = 0.5$; $k_{iu}^{2o} = 0.5$; $k_{iu}^{3o} = 0.5$; $k_{iw}^{1o} = 0.5$; $k_{iw}^{2o} = 0.5$; $k_{iw}^{3o} = 0.5$; $T_{iu} = 5$; $T_{iw} = 5$; $\Delta_{iu} = 1$; $\Delta_{iw} = 1$; $k_{iu}^c = 10$; $k_{iw}^c = 10$.

Conducted by topology in Fig. 2, simulation results are plotted in Figs. 3∼10, where gray bars in Figs. 5∼10 represent the collision avoidance process of each ASV. Specifically, Fig. 3 shows the whole motion trajectories of ASV1∼ASV3 guided by 4 virtual leaders. According to the snapshots at 0s, 200s, 400s, 600s, and 800s, ASV1∼ASV3 converge to the hulls and hold the collision-free cooperative maneuvering pattern. In order to clearly observe the collision avoidance process, Fig. 4 displays the enlarged snapshots, in which ASVs avoid Obstacle1, Obstacle2, and Obstacle3. From Fig. 4(a)-4(b), each ASVs are capable of avoiding the static obstacles (Obstacle1 and Obstacle2). From Fig. 4(c), ASV1 can also avoid the intersection ASV (Obstacle3). The collision-free behaviors in

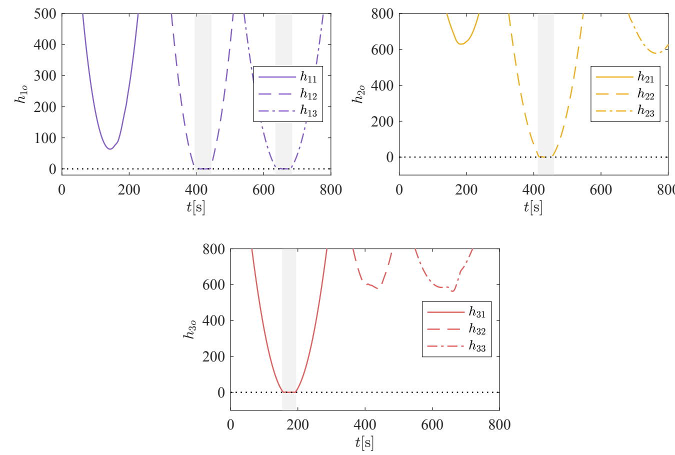

Fig. 5: Second-order CBFs of ASV1∼ASV3 for obstacles.

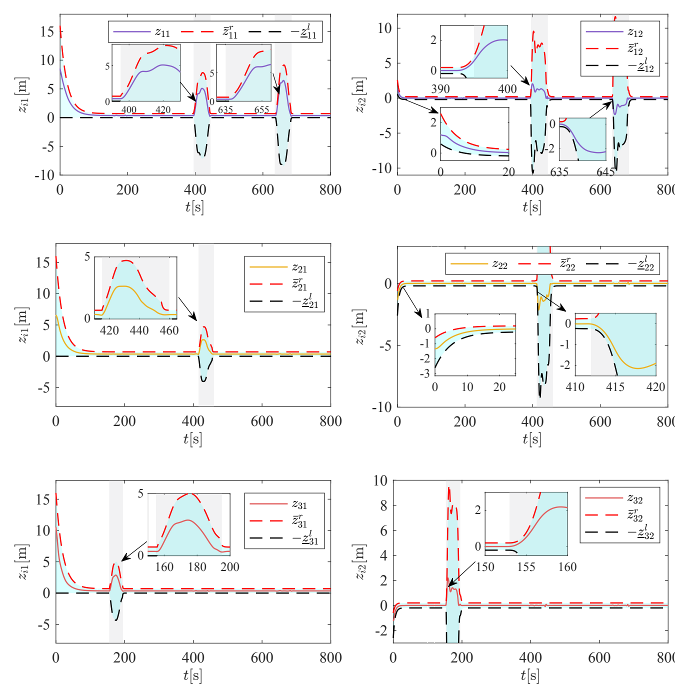

Fig. 6: The relative distances (left column) and heading errors (right column) of all ASVs.

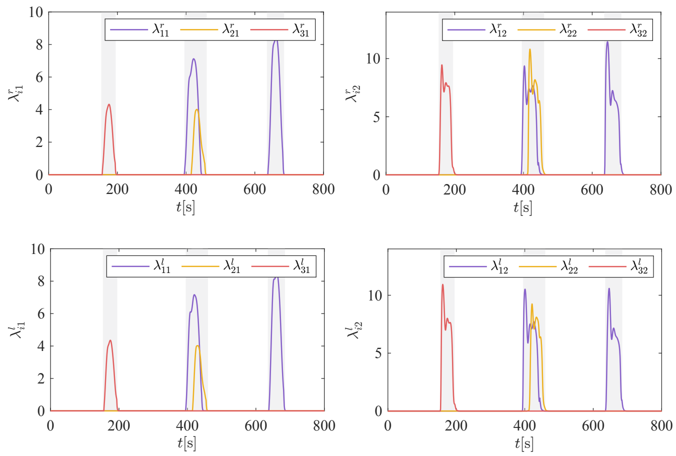

Fig. 7: Auxiliary variables for relative distance and heading errors.

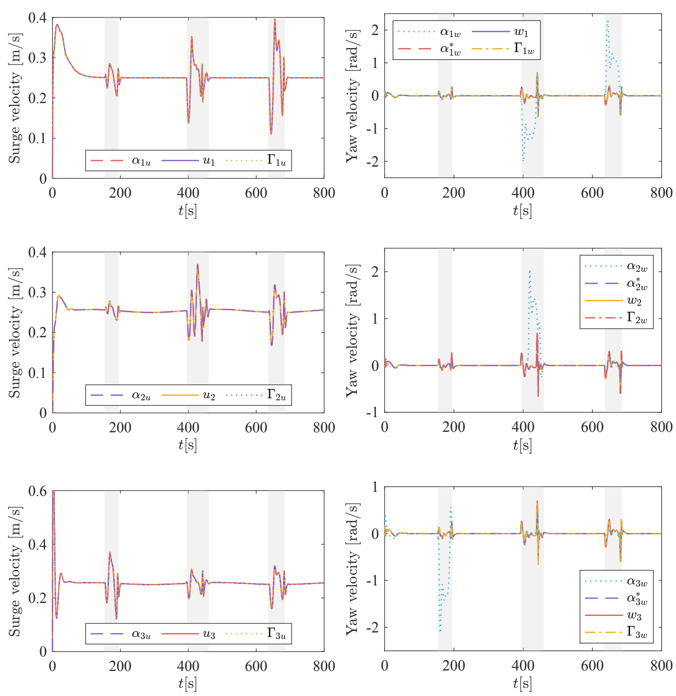

Fig. 8: The surge (left column) and yaw (right column) velocities of all ASVs.

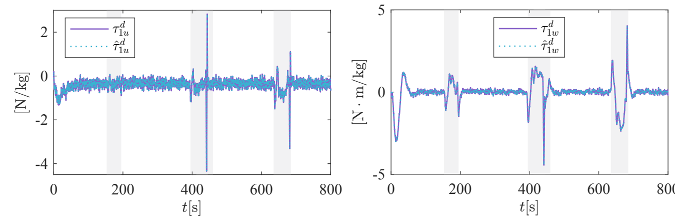

Fig. 9: Estimation performances of PTDO for ASV1.

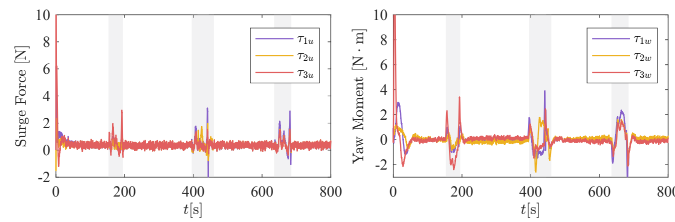

Fig. 10: Properties of control inputs.

Fig. 4 are further verified by the corresponding 2nd-order CBFs for each ASVs in Fig. 5. The non-negativity of $h_{io}(p_i)$ mean that each ASV does not go into the obstacle avoidance zones $\mathcal{C}_{io}(p_i)$, i.e. $p_i \notin \mathcal{C}_{io}(p_i)$. Then, it is concluded that the modified yaw guidance law (36) ensures the collision-free behaviors and achieve the cooperation of ASV1$\sim$ASV3 from Figs. 3 and 4.

From Fig. 6, the relative distances and heading errors of ASV1$\sim$ASV3 can converge into the prescribed constraint spaces $[-\underline{z}^l_{i1}, \bar{z}^r_{i1}]$ and $[-\underline{z}^l_{i2}, \bar{z}^r_{i2}]$. Under the collision-free protocol, z_{i1} escapes from the original constraint space $[-z^l_{i1}, z^r_{i1}]$. To not violate the performance constraints, the space $[-z^l_{i1}, z^r_{i1}]$ are enlarged to $[-\underline{z}^l_{i1}, \bar{z}^r_{i1}]$ with the positive modified signals λ^r_{i1}, λ^l_{i1} from proposed auxiliary system (18). It is seen that the error z_{i1} evolves within the enlarged constraint spaces from Fig. 6(a), 6(c), and 6(e). In addition, it knows that errors z_{12} and z_{22} gently to the prescribed neighboring region of the origin without obvious overshoots from Fig. 6(b), 6(d), and 6(f). Fig. 7draws the modified variables λ^r_{i1}, λ^l_{i1}, λ^r_{i2}, and λ^l_{i2} for relative distances z_{i1} and heading errors z_{i2}, respectively. When it does not avoid collision, the modified variables are at the origin, which means that prescribed performances are not affected. When avoiding collision, the positive modified values are generated to enhance the adaptability of prescribed bounds without changing parameters $\rho_{i1,\infty}$ and $\rho_{i2,\infty}$.

Fig. 8 gives the surge and yaw velocity signals of ASV1$\sim$ASV3, respectively. According to Fig. 8(b), the yaw velocity adjustment in the first gray bar is to hold the cooperation of ASV1$\sim$ASV3 when ASV3 avoids Obstacle1, and the adjustments of the second and third gray bars are due to avoiding Obstacle2 and intersection ASV for ASV1. In Fig. 9, the disturbance estimations for ASV1 in the surge and yaw direction are presented by using the proposed PTDOs. Fig. 10 shows the surge forces and yaw moments of ASV1$\sim$ASV3.

VI. Conclusions

In this paper, we introduce a constrained safe cooperative maneuvering method for multiple underactuated ASVs subject to performance-prescribed and obstacle-loaded constraints. Our proposed method contains a guidance loop and a control loop. In the guidance loop, the designed ATPP can not only achieve the transient and steady-state indices of relative position and heading control but also modify bounds for possible collision avoidance actions of ASVs. The barrier-certified yaw velocity protocol guarantees the safety of multi-ASV system in an obstacle-loaded environment. In the control loop, the PTDO-based kinetic control laws are devised under unknown environmental disturbances. Simulation results of three ASVs verified the efficacy of the constrained safe cooperative maneuvering method. For future study, it is desirable to achieve the constrained safe cooperative control of ASVs with the Convention on the International Regulations for Preventing Collisions at Sea (COLREGs).

References

[1] Z. Peng, J. Wang, D. Wang, and Q. Han, "An overview of recent advances in coordinated control of multiple autonomous surface vehicles," *IEEE Trans. Ind. Informat.*, vol. 17, no. 2, pp. 732–745, 2021.

[2] Y. Shi, C. Shen, H. Fang, and H. Li, "Advanced control in marine mechatronic systems: A survey," *IEEE/ASME Trans. Mechatron.*, vol. 22, no. 3, pp. 1121–1131, 2017.

[3] N. Gu, D. Wang, Z. Peng, J. Wang, and Q.-L. Han, "Advances in line-of-sight guidance for path following of autonomous marine vehicles: An overview," *IEEE Trans. Syst. Man, Cybern., Syst.*, vol. 53, no. 1, pp. 12–28, 2023.

[4] ——, "Disturbance observers and extended state observers for marine vehicles: A survey," *Control Eng. Pract.*, vol. 123, p. 105158, 2022.

[5] W. Wu, Z. Peng, D. Wang, L. Liu, and Q.-L. Han, "Network-based line-of-sight path tracking of underactuated unmanned surface vehicles with experiment results," *IEEE Trans. Cybern.*, vol. 52, no. 10, pp. 10 937 – 10 947, 2022.

[6] P. Wang, K. Yong, M. Chen, and X. Zhang, "Output-feedback flexible performance-based safe formation for underactuated unmanned surface vehicles," *IEEE Trans. Intell. Veh.*, vol. 8, no. 3, pp. 2437–2447, 2022.

[7] T. Li, W. Bai, Q. Liu, Y. Long, and C. L. P. Chen, "Distributed fault-tolerant containment control protocols for the discrete-time multiagent systems via reinforcement learning method," *IEEE Trans. Neural Netw. Learn. Syst.*, vol. 34, no. 8, pp. 3979–3991, 2023.

[8] Z. Peng, Y. Jiang, L. Liu, and Y. Shi, "Path-guided model-free flocking control of unmanned surface vehicles based on concurrent learning extended state observers," *IEEE Trans. Syst. Man, Cybern., Syst.*, vol. 53, no. 8, pp. 4729–4739, 2023.

[9] Y. Jiang, Z. Peng, D. Wang, Y. Yin, and Q.-L. Han, "Cooperative target enclosing of ring-networked under-actuated autonomous surface vehicles based on data-driven fuzzy predictors and extended state observers," *IEEE Trans. Fuzzy Syst.*, vol. 30, no. 7, pp. 2515–2528, 2022.

[10] G. Ferri, A. Munafo, and K. D. LePage, "An autonomous underwater vehicle data-driven control strategy for target tracking," *IEEE J. Ocean. Eng.*, vol. 43, no. 2, pp. 323–343, 2018.

[11] Y. Yang, Y. Xiao, and T. Li, "Attacks on formation control for multiagent systems," *IEEE Trans. Cybern.*, vol. 52, no. 12, pp. 12 805–12 817, 2021.

[12] L. Liu, D. Wang, Z. Peng, and Q.-L. Han, "Distributed path following of multiple under-actuated autonomous surface vehicles based on data-driven neural predictors via integral concurrent learning," *IEEE Trans. Neural Netw. Learn. Syst.*, vol. 32, no. 12, pp. 5334–5344, 2021.

[13] Z. Peng, J. Wang, and D. Wang, "Containment maneuvering of marine surface vehicles with multiple parameterized paths via spatial-temporal decoupling," *IEEE/ASME Trans. Mechatron.*, vol. 22, no. 2, pp. 1026–1036, 2017.

[14] Z. Peng, J. Wang, and D. Wang, "Distributed containment maneuvering of multiple marine vessels via neurodynamics-based output feedback," *IEEE Trans. Ind. Electron.*, vol. 64, no. 5, pp. 3831–3839, 2017.

[15] Y. Zhang, W. Wu, and W. Zhang, "Noncooperative game-based cooperative maneuvering of intelligent surface vehicles via accelerated learning-based neural predictors," *IEEE Trans. Intell. Veh.*, vol. 8, no. 3, pp. 2212–2221, 2023.

[16] M. Li, C. Guo, H. Yu, and Y. Yuan, "Event-triggered containment control of networked underactuated unmanned surface vehicles with finite-time convergence," *Ocean Eng.*, vol. 246, p. 110548, 2022.

[17] W. Wu, Z. Peng, D. Wang, L. Liu, and N. Gu, "Anti-disturbance leader–follower synchronization control of marine vessels for underway replenishment based on robust exact differentiators," *Ocean Eng.*, vol. 248, p. 110686, 2022.

[18] Z.-Q. Liu, Y.-L. Wang, Q.-L. Han, and Y. Yang, "Network-based multiple operating points cooperative dynamic positioning of unmanned surface vehicles," *IEEE ASME Trans. Mechatron.*, vol. 27, no. 6, pp. 5736–5747, 2022.

[19] C. P. Bechlioulis and G. A. Rovithakis, "Robust adaptive control of feedback linearizable mimo nonlinear systems with prescribed performance," *IEEE Trans. Autom. Control*, vol. 53, no. 9, pp. 2090–2099, 2008.

[20] Y. Qu, W. Zhao, Z. Yu, and B. Xiao, "Distributed prescribed performance containment control for unmanned surface vehicles based on disturbance observer," *ISA Trans.*, vol. 125, pp. 699–706, 2022.

[21] Z. Jia, Z. Hu, and W. Zhang, "Adaptive output-feedback control with prescribed performance for trajectory tracking of underactuated surface vessels," *ISA Trans.*, vol. 95, pp. 18–26, 2019.

[22] L. Chen, R. Cui, C. Yang, and W. Yan, "Adaptive neural network control of underactuated surface vessels with guaranteed transient performance: Theory and experimental results," *IEEE Trans. Ind. Electron.*, vol. 67, no. 5, pp. 4024–4035, 2020.

[23] J. Ghommam, M. Saad, and F. Mnif, "Prescribed performances based fuzzy-adaptive output feedback containment control for multiple underactuated surface vessels," *Ocean Eng.*, vol. 249, p. 110898, 2022.

[24] W. Wu, Y. Zhang, W. Zhang, and W. Xie, "Distributed finite-time performance-prescribed time-varying formation control of autonomous surface vehicles with saturated inputs," *Ocean Eng.*, 2022, doi: 10.1016/j.oceaneng.2022.112866.

[25] Y. Lu, X. Xu, L. Qiao, and W. Zhang, "Robust adaptive formation tracking of autonomous surface vehicles with guaranteed performance and actuator faults," *Ocean Eng.*, vol. 237, p. 109592, 2021.

[26] Z.-Q. Liu, Y.-L. Wang, and Q.-L. Han, "Adaptive fault-tolerant trajectory tracking control of twin-propeller non-rudder unmanned surface vehicles," *Ocean. Eng.*, vol. 285, 2023.

[27] W. Wu, R. Ji, W. Zhang, and Y. Zhang, "Transient-reinforced tunnel coordinated control of underactuated marine surface vehicles with actuator faults," *IEEE Trans. Intell. Transp. Syst.*, 2023, doi: 10.1109/TITS.2023.3324346.

[28] G. Zhu, Y. Ma, Z. Li, R. Malekian, and M. Sotelo, "Adaptive neural output feedback control for MSVs with predefined performance," *IEEE Trans. Veh. Technol.*, vol. 70, no. 4, pp. 2994–3006, 2021.

[29] K. D. Do, "Synchronization motion tracking control of multiple underactuated ships with collision avoidance," *IEEE Trans. Ind. Electron.*, vol. 63, no. 5, pp. 2976–2989, 2016.

[30] N. Gu, D. Wang, Z. Peng, T. Li, and S. Tong, "Model-free containment control of underactuated surface vessels under switching topologies based on guiding vector fields and data-driven neural predictors," *IEEE Trans. Cybern.*, vol. 52, no. 10, pp. 10 843–10 854, 2022.

[31] N. Gu, D. Wang, Z. Peng, and L. Liu, "Observer-based finite-time control for distributed path maneuvering of underactuated unmanned surface vehicles with collision avoidance and connectivity preservation," *IEEE Trans. Syst. Man, Cybern., Syst.*, vol. 51, no. 8, pp. 5105–5115, 2019.

[32] B. S. Park and S. J. Yoo, "Connectivity-maintaining and collision-avoiding performance function approach for robust leader–follower formation control of multiple uncertain underactuated surface vessels," *Automatica*, vol. 127, p. 109501, 2021.

[33] S. He, S.-L. Dai, Z. Zhao, T. Zou, and Y. Ma, "UDE-based distributed formation control for MSVs with collision avoidance and connectivity preservation," *IEEE Trans. Ind. Informat.*, 2023, doi: 10.1109/TII.2023.3274234.

[34] S. He, M. Wang, S. Dai, and F. Luo, "Leader-follower formation control of USVs with prescribed performance and collision avoidance," *IEEE Trans. Ind. Informat.*, vol. 15, no. 1, pp. 572–581, 2019.

[35] K. Lu, S.-L. Dai, and X. Jin, "Adaptive angle-constrained enclosing control for multirobot systems using bearing measurements," *IEEE Trans. Autom. Control*, 2023, doi: 10.1109/TAC.2023.3303096.

[36] N. Gu, D. Wang, Z. Peng, and J. Wang, "Safety-critical containment maneuvering of underactuated autonomous surface vehicles based on neurodynamic optimization with control barrier functions," *IEEE Trans. Neural Netw. Learn. Syst.*, vol. 34, no. 6, pp. 2882–2895, 2023.

[37] W. Wu, Z. Peng, L. Liu, and D. Wang, "A general safety-certified cooperative control architecture for interconnected intelligent surface vehicles with applications to vessel train," *IEEE Trans. Intell. Veh.*, vol. 7, no. 3, pp. 627–637, 2022.

[38] W. Wu, Y. Zhang, W. Zhang, and W. Xie, "Output-feedback finite-time safety-critical coordinated control of path-guided marine surface vessels based on neurodynamic optimization," *IEEE Trans. Syst. Man, Cybern., Syst.*, vol. 53, no. 3, pp. 1788–1800, 2023.

[39] Z. Peng, C. Wang, Y. Yin, and J. Wang, "Safety-certified constrained control of maritime autonomous surface ships for automatic berthing," *IEEE Trans. Veh. Technol.*, 2023, doi:10.1109/TVT.2023.3253204.6.

[40] K. D. Do, "Practical control of underactuated ships," *Ocean. Eng.*, vol. 37, no. 13, pp. 1111–1119, 2010.

[41] Z. Zheng, "Moving path following control for a surface vessel with error constraint," *Automatica*, vol. 118, p. 109040, 2020.

[42] C. Hu, R. Wang, F. Yan, and N. Chen, "Robust composite nonlinear feedback path-following control for underactuated surface vessels with

desired-heading amendment," *IEEE Trans. Ind. Electron.*, vol. 63, no. 10, pp. 6386–6394, 2016.

[43] B. Xiao, X. Yang, and X. Huo, "A novel disturbance estimation scheme for formation control of ocean surface vessels," *IEEE Trans. Ind. Electron.*, vol. 64, no. 6, pp. 4994–5003, 2016.

[44] Z. Peng, D. Wang, and J. Wang, "Cooperative dynamic positioning of multiple marine offshore vessels: A modular design," *IEEE/ASME Trans. Mechatron.*, vol. 21, no. 3, pp. 1210–1221, 2016.

[45] J. Zhang, S. Yu, D. Wu, and Y. Yan, "Nonsingular fixed-time terminal sliding mode trajectory tracking control for marine surface vessels with anti-disturbances," *Ocean Eng.*, vol. 217, p. 108158, 2020.

[46] Z. Peng, D. Wang, and J. Wang, "Data-driven adaptive disturbance observers for model-free trajectory tracking control of maritime autonomous surface ships," *IEEE Trans. Neural Netw. Learn. Syst.*, vol. 32, no. 12, pp. 5584–5594, 2021.

[47] Y. Wang, Y. Song, D. J. Hill, and M. Krstic, "Prescribed-time consensus and containment control of networked multiagent systems," *IEEE Trans. Cybern.*, vol. 49, no. 4, pp. 1138–1147, 2018.

[48] K. D. Do, "Synchronization motion tracking control of multiple underactuated ships with collision avoidance," *IEEE Trans. Ind. Electron.*, vol. 63, no. 5, pp. 2976–2989, 2016.

[49] J. Li, G. Zhang, C. Liu, and W. Zhang, "COLREGs-constrained adaptive fuzzy event-triggered control for underactuated surface vessels with the actuator failures," *IEEE Trans. Fuzzy Syst.*, vol. 29, no. 12, pp. 3822–3832, 2020.

[50] X. Xu, P. Cai, Z. Ahmed, V. S. Yellapu, and W. Zhang, "Path planning and dynamic collision avoidance algorithm under colregs via deep reinforcement learning," *Neurocomputing*, vol. 468, pp. 181–197, 2022.

[51] W. Xiao and C. Belta, "High-order control barrier functions," *IEEE Trans. Autom. Control*, vol. 67, no. 7, pp. 3655–3662, 2022.

[52] A. D. Ames, X. Xu, J. W. Grizzle, and P. Tabuada, "Control barrier function based quadratic programs for safety critical systems," *IEEE Trans. Autom. Control*, vol. 62, no. 8, pp. 3861–3876, 2017.

[53] Y. Jiang, Z. Peng, L. Liu, D. Wang, and F. Zhang, "Safety-critical cooperative target enclosing control of autonomous surface vehicles based on finite-time fuzzy predictors and input-to-state safe high order control barrier functions," *IEEE Trans. Fuzzy Syst.*, 2023, doi: 10.1109/TFUZZ.2023.3309706.

[54] G. Li, Z. Yan, and J. Wang, "A one-layer recurrent neural network for constrained nonsmooth invex optimization," *Neural Netw.*, vol. 50, pp. 79–89, 2014.

[55] H. K. Khalil, *Nonlinear Control*. Pearson Education, 2015.

Wentao Wu (Graduated Student Member, IEEE) received the B.E. degree in electrical engineering and automation from Harbin University of Science and Technology, Harbin, China, in 2018. He received the M.E. degree in electrical engineering from Dalian Maritime University, Dalian, China, in 2021. He is currently pursing the Ph.D. degree in electronic information from Shanghai Jiao Tong University, Shanghai, China.

His current research interests include cooperative control, safety-critical control, and constrained control of multiple marine vehicles. Dr. Wu serves as a reviewer of some international journals, such as, IEEE TRANSACTIONS ON SYSTEMS, MAN, AND CYBERNETICS: SYSTEMS, IEEE/CAA JOURNAL OF AUTOMATICA SINICA, IEEE TRANSACTIONS ON INTELLIGENT VEHICLES, IEEE TRANSACTIONS ON INDUSTRIAL ELECTRONICS, etc.

Yibo Zhang (Member, IEEE) received the B.E. degree in marine electronic and electrical engineering and the Ph. D. degree in marine electrical engineering from Dalian Maritime University, Dalian, China, in 2014 and 2021. He is a postdoctoral fellow with the Department of Automation, Shanghai Jiao Tong University.

His current research interests include cooperative control and intelligent control of multi-agent systems and multiple marine vehicles.

Zhenhua Li received the B.S. degree in automation from Harbin University of Science and Technology, Harbin, China, in 2017, and the M.S. degree in control theory and control engineering from Northeastern University, Shenyang, China, in 2020. He is currently pursuing the Eng.D. degree in electronic information at the Department of Automation, Shanghai Jiao Tong University, Shanghai, China.

His research interests include adaptive control, nonlinear systems, observer theory, switched systems and time-delay systems.

Jun-Guo Lu received the B.E. and Ph.D. degrees in control theory and control engineering from the Nanjing University of Science and Technology, Nanjing, China, in 1997 and 2002, respectively.

From 2001 to 2003, he was a Postdoctoral Fellow with the Department of Automation, Shanghai Jiao Tong University, Shanghai, China. In 2003, he joined Shanghai Jiao Tong University, where he is currently a Professor with the Department of Automation. His current research interests include nonlinear output regulation theory and applications, fractional-order control system, robot control and multirobot coordination, machine vision, and three-dimensional digitalization.

Weidong Zhang (Senior Member, IEEE) received his BS, MS, and PhD degrees from Zhejiang University, China, in 1990, 1993, and 1996, respectively, and then worked as a Postdoctoral Fellow at Shanghai Jiaotong University.

He joined Shanghai Jiaotong University in 1998 as an Associate Professor and has been a Full Professor since 1999. From 2003 to 2004 he worked at the University of Stuttgart, Germany, as an Alexander von Humboldt Fellow. He is a recipient of National Science Fund for Distinguished Young Scholars, China and Cheung Kong Scholar, Ministry of Education, China. He is currently Director of the Engineering Research Center of Marine Automation,Shanghai Municipal Education Commission, and Director of Marine Intelligent System Engineering Research Center, Ministry of Education, China. His research interests include control theory, machine learning theory, and their applications in industry and autonomous systems. He is the author of 265 SCI papers and 1 book, and holds 72 patents.